



Naafs, B. D. A., Rohrssen, M., Inglis, G. N., Lähteenoja, O., Feakins, S. J., Collinson, M. E., Kennedy, E. M., Singh, P. K., Singh, M. P., Lunt, D. J., & Pancost, R. D. (2018). High temperatures in the terrestrial mid-latitudes during the early Palaeogene. *Nature Geoscience*, 11, 766–771. <https://doi.org/10.1038/s41561-018-0199-0>

Peer reviewed version

Link to published version (if available):  
[10.1038/s41561-018-0199-0](https://doi.org/10.1038/s41561-018-0199-0)

[Link to publication record in Explore Bristol Research](#)  
PDF-document

This is the author accepted manuscript (AAM). The final published version (version of record) is available online via Nature at <https://www.nature.com/articles/s41561-018-0199-0> . Please refer to any applicable terms of use of the publisher.

## University of Bristol - Explore Bristol Research

### General rights

This document is made available in accordance with publisher policies. Please cite only the published version using the reference above. Full terms of use are available:  
<http://www.bristol.ac.uk/red/research-policy/pure/user-guides/ebr-terms/>

# High temperatures in the terrestrial mid-latitudes during the early Paleogene

B.D.A. Naafs<sup>1\*</sup>, M. Rohrsen<sup>1,2</sup>, G.N. Inglis<sup>1</sup>, O. Lähteenoja<sup>3</sup>, S. J. Feakins<sup>4</sup>, M.E. Collinson<sup>5</sup>, E.M. Kennedy<sup>6</sup>, P.K. Singh<sup>7</sup>, M.P. Singh<sup>7</sup>, D.J. Lunt<sup>8</sup>, R.D. Pancost<sup>1</sup>, and the T-GRES peat database collaborators

<sup>1</sup>Organic Geochemistry Unit, School of Chemistry, School of Earth Sciences, and Cabot Institute, University of Bristol, UK

<sup>2</sup>Department of Earth and Atmospheric Sciences, Central Michigan University, USA

<sup>3</sup>School of Life Sciences, Arizona State University, USA

<sup>4</sup>Department of Earth Sciences, University of Southern California, USA

<sup>5</sup>Department of Earth Sciences, Royal Holloway University of London, UK

<sup>6</sup>Department of Paleontology, GNS Science, Lower Hutt, New Zealand

<sup>7</sup>Coal and Organic Petrology Lab, Department of Geology, Banaras Hindu University, India

<sup>8</sup>School of Geographical Sciences and Cabot Institute, University of Bristol, UK

\* Corresponding author: [david.naafs@bristol.ac.uk](mailto:david.naafs@bristol.ac.uk)

**The early Paleogene (56-48 Myr) provides valuable information about the Earth's climate system in an equilibrium high  $p\text{CO}_2$  world. High ocean temperatures have been reconstructed for this greenhouse period, but land temperature estimates have been cooler than expected. This mismatch between marine and terrestrial temperatures has been difficult to reconcile. Here we present terrestrial temperature estimates from a newly-calibrated *brGDGT*-based paleothermometer in ancient lignites (fossilized peat). Our results suggest early Paleogene mid-latitude (45-60 degrees paleolatitude) mean annual air temperatures of 23 – 29 °C (with an uncertainty of  $\pm 4.7$  °C), 5-10 °C higher than**

most previous estimates. The identification of archaeal biomarkers in these same lignites, heretofore observed only in thermophiles and hyperthermophilic settings, support these high temperature estimates. These mid-latitude terrestrial temperature estimates are consistent with reconstructed ocean temperatures and indicate that the terrestrial realm was much warmer during the early Paleogene than previously thought.

The early Paleogene is characterized by an extended period of high atmospheric carbon dioxide ( $p\text{CO}_2$ ) levels<sup>1,2</sup>. Quantification of temperatures during greenhouse climates is needed 1) because they can be used to evaluate climate model simulations at elevated  $p\text{CO}_2$ <sup>3</sup>, 2) because temperature governs diverse components of climate dynamics (e.g. circulation patterns)<sup>4</sup> and feedback mechanisms within the Earth system (e.g. weathering)<sup>5</sup>, and 3) because they influence biogeochemical processes (e.g. flux of methane from wetlands into the atmosphere)<sup>6</sup>. Although potentially not continuously as hot as the relatively short-lived extreme greenhouse events such as the Paleocene Eocene Thermal Maximum (PETM), the extended greenhouse climate state of the early Paleogene is the focus here.

Over the last decade, considerable effort has been made to reconstruct the early Paleogene greenhouse climate with a variety of calcite-based, leaf physiognomic, and organic geochemical proxies. For example, sea surface temperatures (SSTs) have been reconstructed with the organic TEX<sub>86</sub> proxy<sup>7</sup>, based on the distribution of isoprenoidal glycerol dialkyl glycerol tetraethers (*iso*GDGTs), lipids synthesized by Archaea, in marine sediments. Those records indicate SSTs significantly higher than modern, with SSTs from the SW Pacific at 60 °S paleolatitude above 30 °C<sup>8</sup>. Similarly, calcite-based SST proxies such as the Mg/Ca

ratio or clumped isotopic composition of foraminiferal calcite indicate significantly elevated SSTs at all latitudes during the early Paleogene<sup>9</sup>. Together the SST records indicate ocean temperatures significantly higher than modern with most estimates from between 60 °S and 50 °N above 22 °C (Fig. 1).

Some climate models, such as CCSM3, can (partly) reproduce these elevated temperatures using 16x modern-day  $p\text{CO}_2$  levels<sup>10</sup>, but such  $p\text{CO}_2$  values are higher than proxy estimates for the early Paleogene<sup>1,2</sup>. Other models, such as HadCM3L and ECHAM, generally cannot reproduce the warming at  $p\text{CO}_2$  levels consistent with the marine proxy estimates<sup>3</sup>. The apparent high SST reconstructions have therefore been attributed to proxy complications, such as a subsurface origin of the lipids used in the TEX<sub>86</sub> proxy<sup>11</sup>, variations in early Paleogene seawater chemistry compared to modern that especially influences the calcite-based paleothermometers<sup>12</sup>, and/or a seasonal (summer) bias in the marine proxies<sup>13,14</sup>. However, recent model simulations have identified potential biases against polar warming in general circulation models that are tuned to modern conditions<sup>15,16</sup>, associated with the representation of cloud properties, which may partly explain the model-data discrepancy at mid/high latitudes.

The available terrestrial temperature proxies, based mainly on leaf physiognomic temperature estimates and the MBT(°)/CBT organic mineral soil temperature proxy, based on the distribution of bacterial branched (*br*)GDGTs, suggest that early Paleogene terrestrial temperatures in general were also higher than modern<sup>10,17,18</sup>, but to a lesser degree than indicated by SST reconstructions. There are very few terrestrial temperature data from the (sub)tropics, but almost all estimates indicate mean air temperatures below 22 °C during the early Paleogene at all latitudes (Fig. 1a). These terrestrial temperature estimates are more consistent with climate model simulations<sup>10</sup>, but considerably lower than SST estimates, presenting a



conundrum. In order to understand this greenhouse climate state, independent early Paleogene temperature estimates are needed to test whether temperatures on land were as high as suggested by marine proxies or as low as indicated by most climate model simulations and many existing terrestrial proxies. For this purpose, here we use the distribution of archaeal and bacterial lipids obtained from lignites (ancient peat) to reconstruct temperatures in early Paleogene mid-latitude peatlands.

#### **GDGTs in modern peat**

A decade of research has demonstrated that in mineral soils the degree of methylation of bacterial *br*GDGTs, calculated using the degree of methylation of (5-methyl) branched tetraethers (MBT'<sub>(5me)</sub>) index, is correlated with mean annual air temperature<sup>19,20</sup>. Although temperature is highly correlated with the degree of methylation, the influence of other factors (e.g. nutrient content) is currently poorly constrained among others due to the lack of culture studies. The MBT(°)/CBT mineral soil temperature proxy has been applied to marine sediments to reconstruct early Paleogene terrestrial temperatures<sup>21</sup>. However, the application of the mineral soil calibration to other climatic archives (e.g. peat and by extension lignite) can be problematic as these represent different environmental conditions than those predominantly comprising the modern mineral soil calibration dataset. To address this, a global peat-specific *br*GDGT temperature calibration that is based on MBT'<sub>5me</sub> in a diverse range (n = 470) of modern peats (MAAT<sub>peat</sub>) was recently developed<sup>22</sup>. This proxy has a calibration error of  $\pm 4.7$  °C and reaches saturation at 29.1 °C. It is important to note that in peat settings, MAAT<sub>peat</sub> is unlikely to record seasonal temperatures, because in peats the *br*GDGT pool is dominated by bacterial production at depth below the water table where seasonal temperature fluctuations are muted and

converge to mean annual air temperatures<sup>22</sup>. As with all paleothermometers, we assume that the strong correlation between the degree of methylation of *br*GDGTs and temperature observed in the modern calibration dataset<sup>22</sup> was the same during the early Paleogene.

In addition to Bacteria (that can produce *br*GDGTs), Archaea also live in peat, and their membrane lipids (*iso*GDGTs) are similarly preserved in ancient peat and lignite. Here we examined the *iso*GDGT distribution in our previously compiled global database of modern peat<sup>22</sup>. For the first time, we report *iso*GDGT-5 (as well as *iso*GDGT-6 and -7) in modern mesophilic peats. So far *iso*GDGTs with more than 4 cyclopentane rings have only been found in hot springs and cultures of (acido) hyperthermophiles<sup>23</sup>. It has been suggested that the ability to synthesize *iso*GDGT-5 to 8 is a unique adaption of extremophiles and does not occur in mesophilic settings<sup>23</sup>. However, our work demonstrates that this biomarker is also present in ombrotrophic (acidic) tropical peats located between 20 °S and 20 °N latitude today. *iso*GDGT-5 is only present in significant amounts (>1% of total *iso*GDGT distribution with 1-5 cyclopentane rings) in tropical and ombrotrophic peats with a pH < 5.1 and MAAT > 19.5 °C (Fig. 2). It is absent in all peatlands with a pH > 5.1 or MAAT < 12 °C and present only in trace proportions (<1% of *iso*GDGTs) in acidic peatlands with MAAT between 12°C and 19.5 °C. The highest proportion of *iso*GDGT-5 in the modern database is 9% in an ombrotrophic Indonesian peat (modern MAAT 26.5 °C, pH 3). The distribution of these compounds in modern peats provides strong evidence that their occurrence (when greater than 1% of total *iso*GDGTs with 1-5 cyclopentane rings) is diagnostic for peatlands with high temperatures (>19.5 °C) and low pH (<5.1). We suggest that the proportional abundance of *iso*GDGT-5 (as well as

isoGDGT-6) likely increases with temperature when pH is held constant, although we have insufficient data to convert that into an empirical calibration.

### **Terrestrial temperatures from early Paleogene lignites**

Here we use the relative abundance of the archaeal lipid *iso*GDGT-5 and degree of methylation of bacterial *br*GDGTs ( $MBT'_{5me}$ ) obtained from lignites and newly calibrated proxies using modern peats to reconstruct temperature in early Paleogene peatlands (see SI for details on age models). Ancient peats can be preserved in the form of immature lignites, also known as brown coals, after compaction under low burial pressure and temperatures ( $< 100\text{ }^{\circ}\text{C}$ ). We use lignites from Germany (Schöningen), UK (Cobham), New Zealand (Otaio), and several basins in western India (Barsingsar seam, Bikaner Basin; Kasnau Matasukh seam, Nagaur Basin; Matanomadh and Panandhro seams, Kachchh Basin; and Khadsaliya Clays, Saurashtra Basin). These lignites derive from peatlands influenced by marine incursions and hence reflect local temperature very near sea level.

As far as is possible, given the difficulties of precise dating in purely continental strata, samples deposited within hyperthermals have been avoided (see SI), such that these samples are expected to represent minimum temperature estimates of early Paleogene warmth. However, dating terrestrial sections is difficult and the precise age of all samples, but especially the Indian lignites, remains difficult to confirm, and it remains possible that more extreme climate states have been included.

All latitudes reported here are best estimates for paleolatitudes. Early Paleogene lignites reveal  $MAAT_{peat}$  in Schöningen ( $\sim 46\text{ }^{\circ}\text{N}$ ) varied between  $22.5$  and  $28\text{ }^{\circ}\text{C} \pm 4.7\text{ }^{\circ}\text{C}$  ( $n = 39$ ,  $0.87 < MBT'_{5me} < 0.98$ ) and in Cobham ( $\sim 48\text{ }^{\circ}\text{N}$ ) between  $23.5$  and  $26\text{ }^{\circ}\text{C} \pm 4.7\text{ }^{\circ}\text{C}$  ( $n = 7$ ,  $0.90 < MBT'_{5me} < 0.94$ ) during the latest

Paleocene/earliest Eocene (Fig. 1a). At Otaio (~57 °S) MAAT<sub>peat</sub> in earliest Eocene lignites (i.e. directly following the PETM) varied between 27 and 29 °C ± 4.7 °C (n = 7, 0.91 < MBT'<sub>5me</sub> < 1), close to the upper limit of MAAT<sub>peat</sub>. These mid-latitude temperature reconstructions for the early Paleogene (22 to 29 °C), are markedly warmer than present (2 to 15 °C), even when taking the calibration error of 4.7 °C into account (Fig. 1a). The Indian lignites (~0-5 °N) consist of a variety of lignites of early Paleogene age and are not as well-dated. MAAT<sub>peat</sub> in these lignite samples varied between 28 and 29 °C ± 4.7 °C (n = 9, 0.98 < MBT'<sub>5me</sub> < 1) and were close to the maximum value of the calibration, such that they might be minimum estimates.

All lignites are also associated with the occurrence of archaeal *iso*GDGTs with more than 4 cyclopentane moieties (Fig. 1), predominantly *iso*GDGT-5 but also *iso*GDGT-6 in some samples (see SI). It is unlikely that the presence of these unusual biomarkers is evidence for hyperthermophilic (e.g hot springs) conditions in all of these ancient peatlands. Deep biosphere production of GDGTs during burial at depth is unlikely to be a significant influence on our temperature records as lignite deposits are characterized by low amounts of intact polar lipid GDGTs<sup>24</sup>, arguing against an active GDGT-producing microbial community in such settings.

In the early Paleogene lignites, the abundance of *iso*GDGT-5 is the highest, on average, in India in the palaeotropics; lower values occur between 45-60° paleolatitude (Fig. 1). The high proportions of *iso*GDGT-5 in early Paleogene lignites suggests that acidic peatlands with temperatures higher than 19.5 °C existed at paleolatitudes of 46-48 °N (Cobham and Schöningen) as well as 57 °S (Otaio). Moreover, the proportion of *iso*GDGT-5 in Indian lignites is higher than those found in any modern peat. We suggest that the higher proportions in Indian lignites compared to the other Paleogene sites is not the result of a much lower pH, as there is

independent evidence that at least some of the latter were formed in ombrotrophic *Sphagnum* peats<sup>25</sup>. Instead, it is likely that higher proportions of *iso*GDGT-5 in the Indian lignites indicates MAATs higher than presently found in the low-latitudes.

### **Comparison with existing temperature reconstructions**

Collectively, the entire GDGT biomarker distribution yields two independent temperature estimates that originate from two different domains of life, suggesting that terrestrial peatland temperatures between 45-60° paleolatitude were significantly higher than modern during the early Paleogene period of elevated *p*CO<sub>2</sub>, with values similar to those found at present only in tropical peatlands. Although the bacterial-based MAAT<sub>peat</sub> calibration is near its limit in the Indian lignites, high abundances of *iso*GDGT-5 provide evidence that tropical temperatures were also elevated relative to those of today, consistent with SST reconstructions<sup>9</sup>.

The majority of existing multi-proxy terrestrial temperature data (e.g. foliar physiognomy, MBT<sup>7</sup>/CBT, etc.) suggests that continental temperatures in the mid-latitude Northern Hemisphere (40-60 °N) were below 22 °C during the early Paleogene (**Fig. 1a**). Some leaf physiognomic estimates from the NW America, based mainly on the Kowalski and Dilcher calibration<sup>26</sup> and especially the CLAMP data, suggest temperatures within error to those found at present at these latitudes<sup>10,17</sup>. Similarly, all paleosol-based temperature estimates, obtained using a range of geochemical methods, are close to or below modern-day temperatures at similar latitudes<sup>27</sup>. This is difficult to reconcile given the multi-proxy evidence for significantly elevated *p*CO<sub>2</sub> levels during the early Paleogene<sup>1,2</sup>. Such low temperatures in the mid-latitude Northern Hemisphere are also difficult to reconcile with terrestrial temperatures from the high-latitude Northern Hemisphere (> 60 °N)

that range between 14 and 20 °C<sup>28,29</sup> and widespread evidence of subtropical flora<sup>29,30</sup> and fauna<sup>31,32</sup> in the (high) Arctic.

The MAAT<sub>peat</sub> estimates from the UK and Germany with average values ca. 25 and 27 ± 4.7 °C, respectively, indicate that mid-latitude terrestrial temperatures are at the high end of (or higher than) leaf physiognomic proxy estimates for comparable latitudes (Fig. 1a). However, these new data are consistent with summer temperature estimates in excess of 40 °C based on clumped isotopes of paleosol carbonates from the Bighorn Basin (~45 °N paleolatitude)<sup>33</sup> and δ<sup>18</sup>O-based terrestrial temperatures from mammalian tooth enamel and fish (gar) scales from the southern USA (~30 to 40 °N) with estimates between 28 and 32 ± 5.5 °C<sup>34</sup>. Similarly, the data from Schöningen are consistent with early Eocene temperatures of 22.5 ± 2.5 °C based on leaf margin analysis from the nearby Messel oil shale<sup>35</sup>. These new terrestrial temperature estimates are also consistent with TEX<sub>86</sub>-, Mg/Ca, and clumped isotope-based SST estimates between 19 and 32 °C from the mid-latitude Northern Hemisphere<sup>9,36</sup> (Fig. 1b).

The published early Paleogene terrestrial temperature estimates from between 45 and 65 °S indicate values between ~10 and 20 °C, in general higher than modern values at these latitudes (Fig. 1a). MAAT<sub>peat</sub> estimates from New Zealand are ~ 5-10 °C higher than existing terrestrial temperature estimates for the region, with an average value of 28 ± 4.7 °C. However, some of the existing terrestrial temperature estimates were obtained from marine sediment cores in the Southern Ocean at ~60 °S, but record conditions further south at Wilkes Land (Antarctica) at ~70 °S. They indicate the presence of near-tropical forests on Antarctica<sup>37</sup> and, together with plant microfossil evidence from the Tawanui section in N. Zealand that indicates the presence of thermophilic taxa directly before and after the PETM<sup>38</sup>, they are

consistent with high  $MAAT_{peat}$  values and presence of *isoGDGT-5* in the Otaio lignite. Furthermore,  $MAAT_{peat}$  is consistent with multi-proxy SST estimates from the mid/high latitude Southern Hemisphere that indicate values between 28 and 35 °C<sup>8,9</sup> (Fig. 1b).

It is likely that the  $MAAT_{peat}$  estimates from India of  $28-29 \pm 4.7$  °C represent minimum values, as also indicated by the higher than modern abundance of *isoGDGT-5*. This prevents a direct comparison with published low-latitude SST estimates. Even so, our estimates are slightly higher than terrestrial temperatures currently suggested for the early Paleogene of the Indian subcontinent<sup>39</sup>, but within error of clumped isotope-based SSTs from the coast of India with values of  $30-35 \pm 2.5$  °C<sup>9</sup>.

The offset between some of the existing and  $MAAT_{peat}$  terrestrial temperatures could partly be explained by a potential cold bias in temperatures based on leaf physiognomic and paleosol proxies<sup>10,27</sup>, as well as uncertainty in paleo-elevation of several of the archives, especially those from N. America. We also note that  $MAAT_{peat}$  estimates are higher than most previously published soil MBT'/CBT-based terrestrial temperature estimates from (proximal) marine sediments (Fig. 1a). Although also based on the distribution of *brGDGTs*, MBT'/CBT-based temperatures from marine sediments could be biased by production in the water column or sediments<sup>40</sup>. Marine sediments also represent an integrated temperature across a large catchment area, potentially including a contribution from high altitudes. In addition, recent analytical advances urge for caution in interpreting MBT'/CBT data as the original measurements could be biased by co-eluting compounds<sup>19</sup>. As such, some of the original MBT'/CBT data might not reflect terrestrial temperatures at sea level, explaining the offset with our data.

These lignite-based data therefore reinvigorate the debate about early Paleogene temperatures: we find new evidence for high temperatures on land that are consistent with SST reconstructions, resolving the prior conundrum, but retaining the discrepancies between data and climate model simulations.

### **Comparison with climate model simulations**

There are a number of climate models that have been used to simulate the early Paleogene climate, including CCSM3<sup>10,15,41</sup>, HadCM3L<sup>42</sup>, ECHAM5<sup>43</sup>, FAMOUS<sup>16</sup>, and GISS<sup>44</sup>. Although these climate models originally struggled to simulate warm climates like that of the early Paleogene, especially when using  $p\text{CO}_2$  estimates consistent with proxy-estimates<sup>3</sup>, more recently there has been progress. The latest set of climate model simulations for the early Paleogene (using CCSM3<sup>15</sup> and FAMOUS<sup>16</sup>) provide a better fit with proxy estimates of SSTs using  $p\text{CO}_2$  estimates that are consistent with proxy data after changing specific model parameters such as cloud properties, although they still struggle to reach the extent of warming indicated by SST proxies in the SW Pacific. Crucially, for the mid-latitude Northern Hemisphere (45-50 °N) the latest set of climate models fit the  $\text{MAAT}_{\text{peat}}$  temperature data, but are 5-10 °C warmer than most of the published mid-latitude temperature data (see Fig. 3b).

However, for the mid-latitude Southern Hemisphere (55-60 °S), the magnitude of warming simulated by all climate models is still less than indicated by  $\text{MAAT}_{\text{peat}}$  (Fig. 3a) and published SST estimates<sup>8,45</sup>. This could suggest that climate models are still missing crucial processes. However, it is important to highlight that virtually all mid/high-latitude Southern Hemisphere SST and terrestrial data (including the new  $\text{MAAT}_{\text{peat}}$  data from Otaio) come from the SW Pacific and Pacific sector of the



Southern Ocean. As such, the high temperatures so far found in the mid/high latitude Southern Hemisphere might reflect local conditions and not be fully representative of zonal averages<sup>46</sup>. Future terrestrial temperature estimates using early Paleogene lignites from for example S. America might be able to shed new light on whether these high temperatures were present throughout the mid/high latitude Southern Hemisphere.

These novel terrestrial temperature estimates have important climatic and biogeochemical implications. For example, studies across microbial to ecosystem scales have demonstrated that methanogenesis rates in peatlands and emission of methane to the atmosphere increase significantly with increasing temperature<sup>6,47</sup>. Combined with evidence that indicates that high  $p\text{CO}_2$  would have stimulated primary productivity<sup>48</sup>, our temperature estimates further suggest that the methane flux for a given areal extent of peatland between 45-60 degree paleolatitude could have been much greater during the early Paleogene than at present. As methane is a potent greenhouse gas, our results support previous modeling work<sup>48,49</sup> indicating the presence of an additional positive feedback mechanism associated with extensive warm mid-latitude peats in a high- $\text{CO}_2$  world that could amplify warming to a greater degree than that estimated using existing or GCM-derived temperature estimates.

## References

- 1 Anagnostou, E. *et al.* Changing atmospheric  $\text{CO}_2$  concentration was the primary driver of early Cenozoic climate. *Nature* **533**, 380-384 (2016).
- 2 Beerling, D. J. & Royer, D. L. Convergent Cenozoic  $\text{CO}_2$  history. *Nature Geosci.* **4**, 418-420 (2011).
- 3 Lunt, D. J. *et al.* A model–data comparison for a multi-model ensemble of early Eocene atmosphere–ocean simulations: EoMIP. *Clim. Past* **8**, 1717-1736 (2012).
- 4 IPCC. in *Fifth Assessment Report of the Intergovernmental Panel on Climate Change* (eds T. F. Stocker *et al.*) 1535 (Cambridge University Press, 2013).

306 5 White, A. F. & Blum, A. E. Effects of climate on chemical weathering in  
307 watersheds. *Geochim. Cosmochim. Acta* **59**, 1729-1747 (1995).

308 6 Yvon-Durocher, G. *et al.* Methane fluxes show consistent temperature  
309 dependence across microbial to ecosystem scales. *Nature* **507**, 488-491  
310 (2014).

311 7 Schouten, S., Hopmans, E. C., Schefuss, E. & Sinninghe Damsté, J. S.  
312 Distributional variations in marine crenarchaeotal membrane lipids: a new tool  
313 for reconstructing ancient sea water temperatures? *Earth Planet. Sc. Lett.* **204**,  
314 265-274 (2002).

315 8 Bijl, P. K. *et al.* Early Palaeogene temperature evolution of the southwest  
316 Pacific Ocean. *Nature* **461**, 776-779 (2009).

317 9 Evans, D. *et al.* Eocene greenhouse climate revealed by coupled clumped  
318 isotope-Mg/Ca thermometry. *P. Natl. Acad. Sci. USA* **PNAS Early Edition**  
319 (2018).

320 10 Huber, M. & Caballero, R. The early Eocene equable climate problem  
321 revisited. *Clim. Past* **7**, 603-633 (2011).

322 11 Ho, S. L. & Laepple, T. Flat meridional temperature gradient in the early  
323 Eocene in the subsurface rather than surface ocean. *Nature Geosci.* **9**, 606-610  
324 (2016).

325 12 Evans, D. & Müller, W. Deep time foraminifera Mg/Ca paleothermometry:  
326 Nonlinear correction for secular change in seawater Mg/Ca.  
327 *Paleoceanography* **27**, PA4205 (2012).

328 13 Eberle, J. J. *et al.* Seasonal variability in Arctic temperatures during early  
329 Eocene time. *Earth Planet. Sc. Lett.* **296**, 481-486 (2010).

330 14 Hollis, C. J. *et al.* Early Paleogene temperature history of the Southwest  
331 Pacific Ocean: Reconciling proxies and models. *Earth Planet. Sc. Lett.* **349–**  
332 **350**, 53-66 (2012).

333 15 Kiehl, J. T. & Shields, C. A. Sensitivity of the Palaeocene–Eocene Thermal  
334 Maximum climate to cloud properties. *Philos. T. Roy. Soc. A* **371**, 0093  
335 (2013).

336 16 Sagoo, N., Valdes, P., Flecker, R. & Gregoire, L. J. The Early Eocene equable  
337 climate problem: can perturbations of climate model parameters identify  
338 possible solutions? *Philos. T. Roy. Soc. A* **371**, 0123 (2013).

339 17 Yang, J., Spicer, R. A., Spicer, T. E. V. & Li, C.-S. ‘CLAMP Online’: a new  
340 web-based palaeoclimate tool and its application to the terrestrial Paleogene  
341 and Neogene of North America. *Palaeobiodivers. palaeoenviro.* **91**, 163-183  
342 (2011).

343 18 Inglis, G. N. *et al.* Mid-latitude continental temperatures through the early  
344 Eocene in western Europe. *Earth Planet. Sc. Lett.* **460**, 86-96 (2017).

345 19 De Jonge, C. *et al.* Occurrence and abundance of 6-methyl branched glycerol  
346 dialkyl glycerol tetraethers in soils: implications for palaeoclimate  
347 reconstruction. *Geochim. Cosmochim. Acta* **141**, 97-112 (2014).

348 20 Weijers, J. W. H., Schouten, S., van den Donker, J. C., Hopmans, E. C. &  
349 Sinninghe Damsté, J. S. Environmental controls on bacterial tetraether  
350 membrane lipid distribution in soils. *Geochim. Cosmochim. Acta* **71**, 703-713  
351 (2007).

352 21 Pancost, R. D. *et al.* Early Paleogene evolution of terrestrial climate in the SW  
353 Pacific, Southern New Zealand. *Geochim. Geophys. Geosyst.* **14**, 5413-5429  
354 (2013).

- 355 22 Naafs, B. D. A. *et al.* Introducing global peat-specific temperature and pH  
356 calibrations based on brGDGT bacterial lipids. *Geochim. Cosmochim. Acta*  
357 **208**, 285-301 (2017).
- 358 23 Schouten, S., Hopmans, E. C. & Sinninghe Damsté, J. S. The organic  
359 geochemistry of glycerol dialkyl glycerol tetraether lipids: A review. *Org.*  
360 *Geochem.* **54**, 19-61 (2013).
- 361 24 Fry, J. C. *et al.* Prokaryotic Populations and Activities in an Interbedded Coal  
362 Deposit, Including a Previously Deeply Buried Section (1.6–2.3 km) Above ~  
363 150 Ma Basement Rock. *Geomicrobiol. J.* **26**, 163-178 (2009).
- 364 25 Inglis, G. N. *et al.* Ecological and biogeochemical change in an early  
365 Paleogene peat-forming environment: Linking biomarkers and palynology.  
366 *Palaeogeogr. Palaeoclimatol. Palaeoecol.* **438**, 245-255 (2015).
- 367 26 Kowalski, E. A. & Dilcher, D. L. Warmer paleotemperatures for terrestrial  
368 ecosystems. *Proc. Natl. Acad. Sci.* **100**, 167-170 (2003).
- 369 27 Hyland, E., Sheldon, N. D. & Fan, M. Terrestrial paleoenvironmental  
370 reconstructions indicate transient peak warming during the early Eocene  
371 climatic optimum. *Geol. Soc. Am. Bull.* **125**, 1338-1348 (2013).
- 372 28 Weijers, J. W. H., Schouten, S., Sluijs, A., Brinkhuis, H. & Sinninghe Damsté,  
373 J. S. Warm arctic continents during the Palaeocene–Eocene thermal  
374 maximum. *Earth Planet. Sc. Lett.* **261**, 230-238 (2007).
- 375 29 Suan, G. *et al.* Subtropical climate conditions and mangrove growth in Arctic  
376 Siberia during the early Eocene. *Geology* **45**, 539-542 (2017).
- 377 30 Sluijs, A. *et al.* Warm and wet conditions in the Arctic region during Eocene  
378 Thermal Maximum 2. *Nature Geosci.* **2**, 777-780 (2009).
- 379 31 Eberle, J. J. & Greenwood, D. R. Life at the top of the greenhouse Eocene  
380 world—A review of the Eocene flora and vertebrate fauna from Canada's  
381 High Arctic. *Geol. Soc. Am. Bull.* **124**, 3-23 (2012).
- 382 32 Dawson, M. R., West, R. M., Langston, W. & Hutchison, J. H. Paleogene  
383 Terrestrial Vertebrates: Northernmost Occurrence, Ellesmere Island, Canada.  
384 *Science* **192**, 781 (1976).
- 385 33 Snell, K. E. *et al.* Hot summers in the Bighorn Basin during the early  
386 Paleogene. *Geology* **41**, 55-58 (2013).
- 387 34 Fricke, H. C. & Wing, S. L. Oxygen isotope and paleobotanical estimates of  
388 temperature and  $\delta^{18}\text{O}$ –latitude gradients over North America during the early  
389 Eocene. *Am. J. Sci.* **304**, 612-635 (2004).
- 390 35 Grein, M., Konrad, W., Wilde, V., Utescher, T. & Roth-Nebelsick, A.  
391 Reconstruction of atmospheric CO<sub>2</sub> during the early middle Eocene by  
392 application of a gas exchange model to fossil plants from the Messel  
393 Formation, Germany. *Palaeogeogr. Palaeoclimatol. Palaeoecol.* **309**, 383-391  
394 (2011).
- 395 36 Sluijs, A. *et al.* Environmental precursors to rapid light carbon injection at the  
396 Palaeocene/Eocene boundary. *Nature* **450**, 1218-1221 (2007).
- 397 37 Pross, J. *et al.* Persistent near-tropical warmth on the Antarctic continent  
398 during the early Eocene epoch. *Nature* **488**, 73-77 (2012).
- 399 38 Crouch, E. M. & Visscher, H. Terrestrial vegetation record across the initial  
400 Eocene thermal maximum at the Tawanui marine section, New Zealand. *Spec.*  
401 *Pap./Geol. Soc. Am.* **369**, 351-363 (2003).
- 402 39 Spicer, R. A. *et al.* Asian Eocene monsoons as revealed by leaf architectural  
403 signatures. *Earth Planet. Sc. Lett.* **449**, 61-68 (2016).

- 404 40 Sinninghe Damsté, J. S. Spatial heterogeneity of sources of branched  
405 tetraethers in shelf systems: The geochemistry of tetraethers in the Berau  
406 River delta (Kalimantan, Indonesia). *Geochim. Cosmochim. Acta* **186**, 13-31  
407 (2016).
- 408 41 Winguth, A., Shellito, C., Shields, C. & Winguth, C. Climate Response at the  
409 Paleocene–Eocene Thermal Maximum to Greenhouse Gas Forcing—A Model  
410 Study with CCSM3. *J. Climate* **23**, 2562-2584 (2009).
- 411 42 Lunt, D. J. *et al.* CO<sub>2</sub>-driven ocean circulation changes as an amplifier of  
412 Paleocene-Eocene thermal maximum hydrate destabilization. *Geology* **38**,  
413 875-878 (2010).
- 414 43 Heinemann, M., Jungclauss, J. H. & Marotzke, J. Warm Paleocene/Eocene  
415 climate as simulated in ECHAM5/MPI-OM. *Clim. Past* **5**, 785-802 (2009).
- 416 44 Roberts, C. D., LeGrande, A. N. & Tripathi, A. K. Climate sensitivity to Arctic  
417 seaway restriction during the early Paleogene. *Earth Planet. Sc. Lett.* **286**, 576-  
418 585 (2009).
- 419 45 Creech, J. B., Baker, J. A., Hollis, C. J., Morgans, H. E. G. & Smith, E. G. C.  
420 Eocene sea temperatures for the mid-latitude southwest Pacific from Mg/Ca  
421 ratios in planktonic and benthic foraminifera. *Earth Planet. Sc. Lett.* **299**, 483-  
422 495 (2010).
- 423 46 Douglas, P. M. J. *et al.* Pronounced zonal heterogeneity in Eocene southern  
424 high-latitude sea surface temperatures. *P. Natl. Acad. Sci. USA* **111**, 6582-  
425 6587 (2014).
- 426 47 Cao, M., Gregson, K. & Marshall, S. Global methane emission from wetlands  
427 and its sensitivity to climate change. *Atmos. Environ.* **32**, 3293-3299 (1998).
- 428 48 Beerling, D. J., Fox, A., Stevenson, D. S. & Valdes, P. J. Enhanced chemistry-  
429 climate feedbacks in past greenhouse worlds. *P. Natl. Acad. Sci. USA* **108**,  
430 9770-9775 (2011).
- 431 49 Sloan, L. C., Walker, J. C. G., Moore, T. C., Rea, D. K. & Zachos, J. C.  
432 Possible methane-induced polar warming in the early Eocene. *Nature* **357**,  
433 320-322 (1992).

## 436 Acknowledgements

437 The research leading to these results has received funding from the European  
438 Research Council under the European Union's Seventh Framework Programme  
439 (FP/2007-2013) / ERC Grant Agreement number 340923 (T-GRES, awarded to  
440 RDP). RDP also acknowledges the Royal Society Wolfson Research Merit Award.  
441 MR received support from the Agouron Institute geobiology postdoctoral research  
442 fellowship. EMK was supported by the New Zealand government funded Global  
443 Change through Time Programme at GNS Science. Cobham and Schoningen samples  
444 were originally collected for other research projects and we particularly thank Volker

Wilde and Walter Riegel (Schöningen) and Jerry Hooker (Cobham) for their extensive personal support during sample collection. Schöningen samples were collected with logistical and financial support that includes NERC grants numbers NE/J008656/1 to MEC and NE/J008591/1 to RDP and we thank ‘Helmstedter Revier of MIBRAG’ and previous owners for access to the mine which has now closed. Alfred McAlpine, AMEC, and Channel Tunnel Rail Link are thanked for providing access to the Cobham site. We thank A. Farnsworth for calculating the paleolatitudes for all locations.

#### **Author contributions**

BDAN, MEC, and RDP designed the project. BDAN analyzed all samples in the modern peat database for *iso*GDGTs and wrote the manuscript with contributions from all authors. MR analyzed the Indian and Otaio lignite samples for GDGTs, while GNI analyzed the Cobham and Schöningen lignite samples for GDGTs. BDAN, MEC and EMK developed the database of early Paleogene terrestrial palaeoclimate proxies. MEC (Cobham and Schöningen samples), EMK (Otaio samples) and PKS (Indian samples) provided age models and stratigraphic context of lignites. OL provided the modern tropical peat samples from Peru.

The T-GRES peat database collaboration consists of: B.D.A. Naafs, G.N. Inglis, Y. Zheng, M.J. Amesbury, H. Biester, R. Bindler, J. Blewett, M.A. Burrows, D. del Castillo Torres, F.M. Chambers, A.D. Cohen, R.P. Evershed, S.J. Feakins, M. Galka, A. Gallego-Sala, L. Gandois, D.M. Gray, P.G. Hatcher, E.N. Honorio Coronado, P.D.M. Hughes, A. Huguet, M. Könönen, F. Laggoun-Défarge, O. Lähteenoja, M. Lamentowicz, R. Marchant, E. McClymont, X. Pontevedra-Pombal,

C. Ponton, A. Pourmand, A.M. Rizzuti, L. Rochefort, J. Schellekens, F. De  
Vleeschouwer, and R.D. Pancost.

## **Financial and non-financial competing interests**

The authors declare no competing financial interests

## **Figure Captions**

### **Fig. 1: early Paleogene temperature**

a) MAAT<sub>peat</sub> (stars) and abundance of *iso*GDGT-5 in early Paleogene lignites (bar chart) together with published temperatures using leaf physiognomy (green squares), MBT'/CBT proxy (dark circles), paleosol proxies (purple diamonds), and mammalian  $\delta^{18}\text{O}$  (violet crosses). b) MAAT<sub>peat</sub> and abundance of *iso*GDGT-5 with published TEX<sub>86</sub>/BAYSPAR-based (blue circles) and calcite-based SSTs (triangles) for the early Paleogene. Error bars on temperature data reflect combined spread in data ( $1\sigma$ ) and calibration uncertainty (SI), while those for *iso*GDGT-5 reflect  $1\sigma$  from the average. All data and references are in the SI. Small grey circles and squares represents modern-day terrestrial and marine temperatures, respectively.

### **Fig. 2: *iso*GDGT in modern peats**

Maximum relative abundance of *iso*GDGT-5 in modern peats plotted against *in situ* peat pH<sup>22</sup> and mean annual air temperature<sup>22</sup>. Vertical bars reflect range in pH reported for each peat. Shaded area indicates tropical ombrotrophic peats characterized by an *iso*GDGT-5 abundance > 1%.

### **Fig. 3: data-model comparison for the early Paleogene**

494 Temperature anomaly between the early Paleogene and present at the paleolatitude of  
495 each location for all terrestrial temperature data from a) between 55 and 60 °S and b)  
496 from between 45 and 50 °N. Error bars reflect combined spread in data ( $1\sigma$ ) and  
497 calibration uncertainty (see SI for details). Also shown is the zonal mean anomaly  
498 (early Paleogene minus pre-industrial) simulated by a range of climate models; 2xCO<sub>2</sub>  
499 ECHAM5<sup>43</sup>, 2xCO<sub>2</sub> FAMOUS<sup>16</sup>, 4xCO<sub>2</sub> GISS<sup>44</sup>, 5xCO<sub>2</sub> CCSM3\_K<sup>15</sup>, 6xCO<sub>2</sub>  
500 HadCM3L<sup>42</sup>, 16xCO<sub>2</sub> CCSM3\_W<sup>41</sup> and 16xCO<sub>2</sub> CCSM3\_H<sup>10</sup> (see SI).

## 501   **Methods**

502   The biomarkers from the lignites from Schöningen were previously extracted<sup>18</sup>. For  
503   this purpose approximately 0.5-10 g of sediment were extracted via Soxhlet apparatus  
504   for 24 hours using dichloromethane:methanol (DCM:MeOH; 2:1 v/v) to yield a total  
505   lipid extract (TLE). The TLE was initially separated over silica into neutral and fatty  
506   acid fractions using chloroform-saturated ammonia and chloroform:acetic acid (100:1  
507   v/v), respectively. The neutral fraction was subsequently fractionated over alumina  
508   into apolar and polar (containing the GDGTs) fractions using Hexane:DCM (9:1 v/v)  
509   and DCM:MeOH (1:2 v/v), respectively. The biomarkers from the Cobham lignite  
510   were previously extracted<sup>50</sup>. For this purpose samples were extracted by sonication  
511   with a sequence of increasingly polar solvents (four times with dichloromethane  
512   (DCM), four times with DCM/methanol (1:1 v/v) and three times with methanol). The  
513   total lipid extracts were separated into three fractions using a column packed with  
514   (activated) alumina by elution with hexane (apolar fraction), hexane/DCM (9:1 v/v; 3  
515   ml) and DCM/methanol (1:2 v/v; 3 ml; polar fraction). Lignites from New Zealand  
516   were extracted for 24h in Soxhlet using DCM:MeOH, (2:1 v/v) and separated over  
517   alumina into apolar (hexane:DCM, 9:1 v/v) and polar (DCM:MeOH, 1:2 v/v)  
518   fractions. TLEs from Indian lignites were obtained via microwave extraction  
519   (Milestone Inc., CT, USA) using DCM:MeOH (9:1 v/v) for 10 minutes at 70°C.  
520   Aliquots of TLE were separated into hydrocarbon (hexane), aromatic (hexane:DCM,  
521   1:1 v/v), and polar fractions (DCM:MeOH 3:1 v/v) over silica.

522         For all samples the polar fraction was dissolved in hexane/*iso*-propanol (99:1,  
523   v/v) and passed through 0.45µm PTFE filters. Fractions were analyzed by high  
524   performance liquid chromatography/atmospheric pressure chemical ionisation – mass  
525   spectrometry (HPLC/APCI-MS). Instrument methods followed Hopmans et al.<sup>51</sup>.



Analyses were performed in selective ion monitoring (SIM) mode to increase sensitivity and reproducibility, and M+H<sup>+</sup> (protonated molecular ion) GDGT peaks were integrated.

Mean annual air temperatures for the lignites were obtained using the degree of methylation of *br*GDGTs as reflected in the MBT'<sub>5me</sub> index<sup>19</sup> and MAAT<sub>peat</sub> calibration<sup>22</sup> (see SI for additional information).

$$MBT'_{5ME}$$

$$= \frac{(brGDGT - Ia + brGDGT - Ib + brGDGT - Ic)}{(brGDGT - Ia + brGDGT - Ib + brGDGT - Ic + brGDGT - IIa + brGDGT - IIb + brGDGT - IIc)}$$

$$MAAT_{peat} (^{\circ}C) = 52.18 \times MBT'_{5me} - 23.05$$

*iso*GDGT-5 was identified based on relative retention times, as well as co-injection with an acid hydrolyzed >95% pure culture of the thermoacidophile *Thermoplasma acidophilum* (Matreya) (see SI). The relative abundance of *iso*GDGT-5 was calculated using the respective peak areas of *iso*GDGTs with one, two, three, and five cyclopentane rings;

$$(1) \text{ } isoGDGT - 5 (\%)$$

$$= 100 \times \frac{(isoGDGT - 5)}{(isoGDGT - 1) + (isoGDGT - 2) + (isoGDGT - 3) + (isoGDGT - 5)}$$

*Iso*GDGT-4 was excluded from this ratio due to the co-elution with the [M+H]<sup>+</sup> + 2 ion of crenarchaeol that also gives *m/z* 1294<sup>52</sup>.

## Data availability

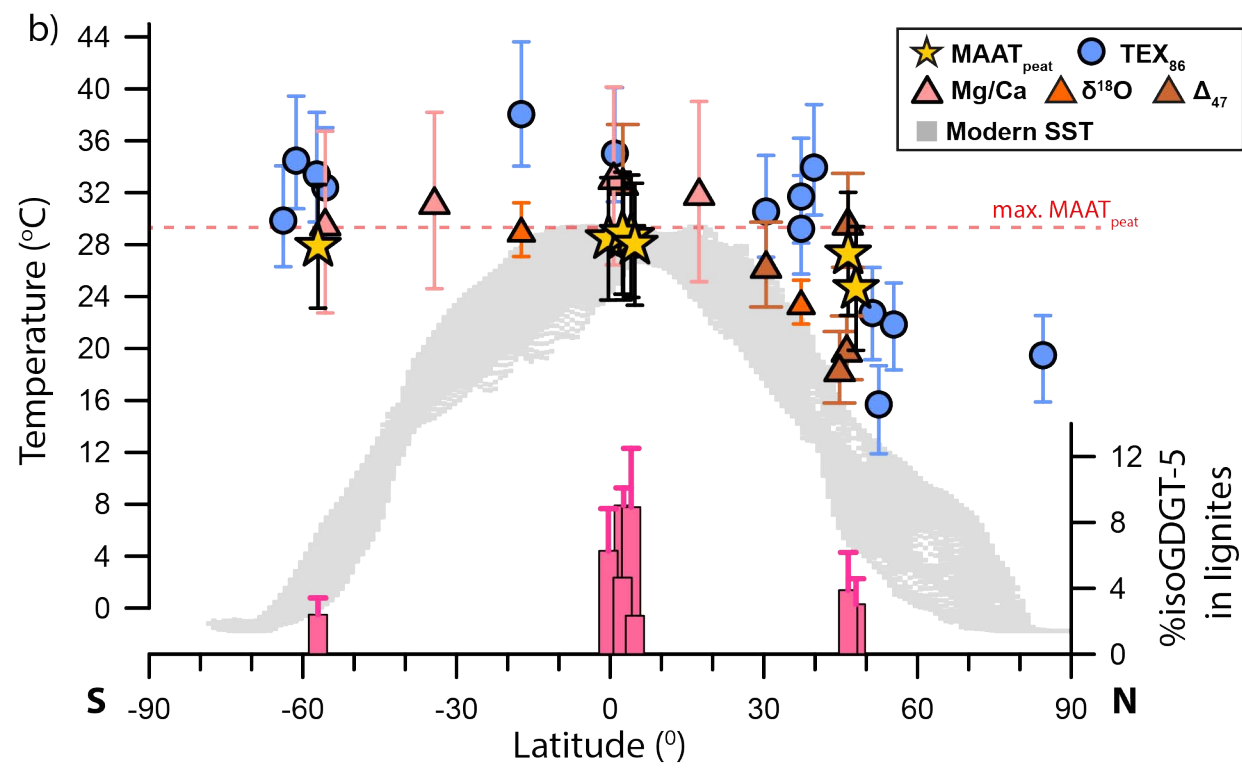
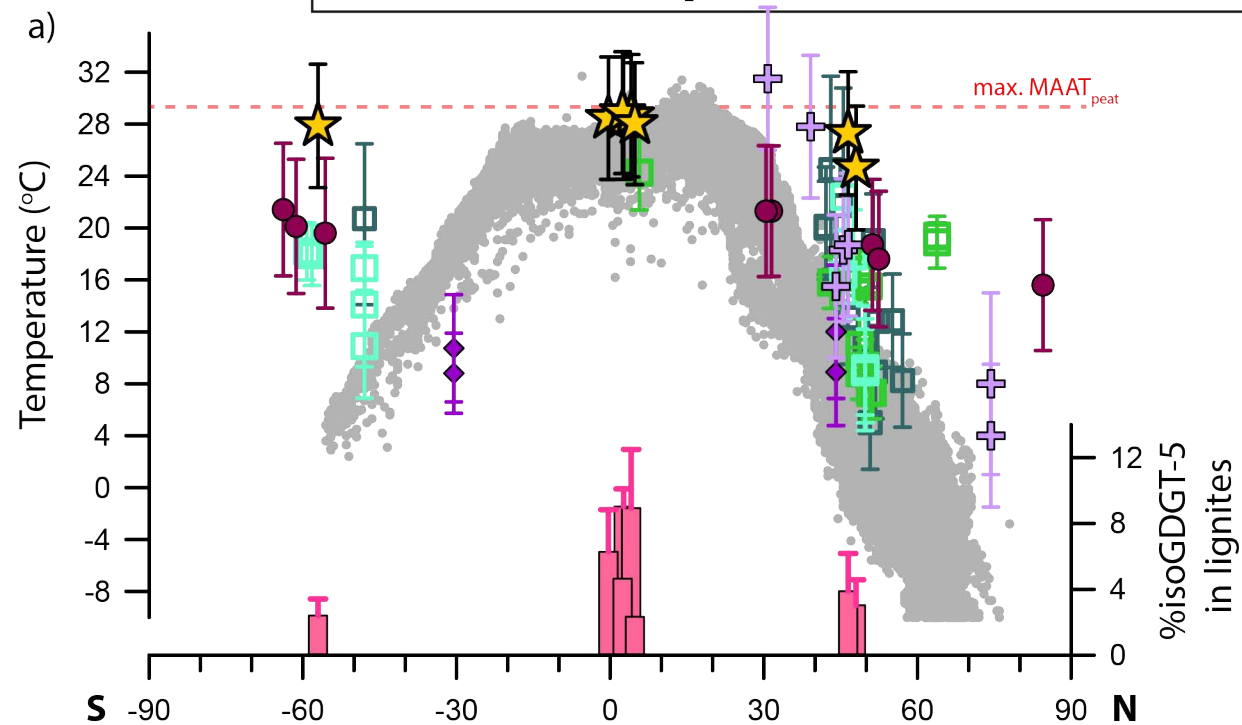
The authors declare that all data supporting the findings of this study are available within the article (and its supplementary information files and the Pangaea database). All data are available in the supplements and in addition all modern peat GDGT data are available on the Pangaea database <https://doi.org/10.1594/PANGAEA.883765> as

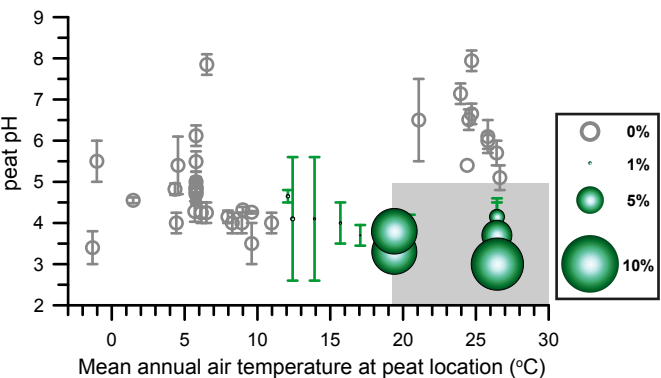
550 [well](#). The compilation of all previously published terrestrial and marine temperature  
551 data from the early Paleogene together with the original references is also available in  
552 the supplements.

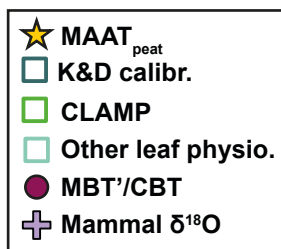
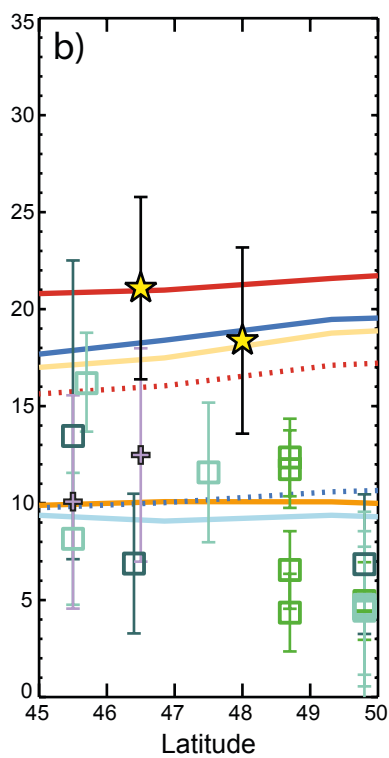
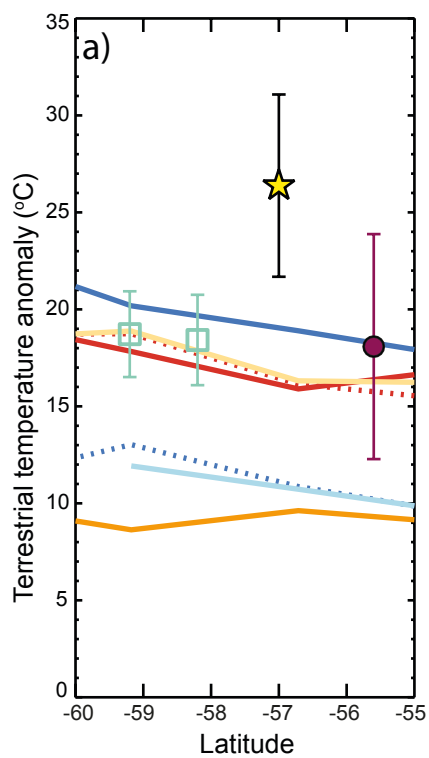
553

#### 554 **References**

- 555 50 Pancost, R. D. *et al.* Increased terrestrial methane cycling at the Palaeocene-  
556 Eocene thermal maximum. *Nature* **449**, 332-335 (2007).  
557 51 Hopmans, E. C., Schouten, S. & Sinninghe Damsté, J. S. The effect of  
558 improved chromatography on GDGT-based palaeoproxies. *Org. Geochem.* **93**,  
559 1-6 (2016).  
560 52 Weijers, J. W. H., Schouten, S., van der Linden, M., van Geel, B. & Sinninghe  
561 Damsté, J. S. Water table related variations in the abundance of intact archaeal  
562 membrane lipids in a Swedish peat bog. *FEMS Microbiol. Lett.* **239**, 51-56  
563 (2004).  
564







Supplementary information to *High temperatures in the terrestrial mid-latitudes during the early Paleogene* by Naafs et al.

**1. Description of lignites and age models**

**1.1 Schöningen lignite (Germany)**

36 samples were collected from Seam 1 in the Schöningen Südfeld mine, northern Germany (51.13°N, 11.00°E) (Fig. S1). Samples no. 33 to 1 were obtained from the high-resolution sampling series of 2008 and 2012<sup>S1,2</sup>. Samples XXIII 4a to XXXIII 7b were obtained from subsequent low-resolution sampling<sup>S2</sup>. The lignites in this mine were deposited as peat in a low lying coastal setting<sup>S3</sup> with a paleolatitude of around 46 °N. The seam from which the samples are derived is ~2.7 m thick and is overlain and underlain by brackish to shallow marine, clastic sedimentary deposits<sup>S3,4</sup>.

The dinocyst zone D 5nb was recognized above the Main Seam in the nearby Emmerstedt area by Ahrendt et al.<sup>S5</sup>. If the Main seam is coeval at both sites this would indicate that Seam 1 at Schöningen is earliest Eocene. However, within marine Interbed 2, directly above Seam 1, there is a dramatic increase in the abundance of the dinocyst *Apectodinium*<sup>S3</sup> which may represent the onset of the Paleocene-Eocene Thermal Maximum (PETM) as it does at other sites<sup>S6,7</sup>. However, none of the studied samples yielded a negative  $\delta^{13}\text{C}$  excursion that would suggest it was deposited during the main body of the PETM<sup>S4</sup>. Therefore, Seam 1 is considered to be either very latest Paleocene or very earliest Eocene in age. During the subsequent early Eocene (Seam 3 upwards), there is a long-term temperature maximum recorded from both the lignites and nearshore marine interbeds, consistent with changes in the palynological assemblage<sup>S2,3</sup>. As this interval may include the Early Eocene Climatic Optimum (EECO)<sup>S1</sup>, this suggests that Seam 1 was deposited prior to the EECO. Further details of sample positions and the lignite sequence at Schöningen can be found in the supplementary material to Robson et al.<sup>S1</sup> and Inglis et al.<sup>S2</sup>.

**1.2 Cobham lignite (UK)**

A total of 7 samples were used from the Cobham Lignite Bed at Cobham, UK (51.40°N, 0.40°E). Samples were obtained from previous sampling events<sup>S8</sup>. This lignite was deposited in a low-lying freshwater setting at the southwest shore (very near sea-level) of the North Sea (~48 °N palaeolatitude)<sup>S9,10</sup>. The Cobham Lignite Bed

at Cobham comprises a thin clay layer (<3 cm) at the base, overlain by a laminated lignite (~55 cm thick). This is succeeded by another thin clay layer (<10 cm) and overlain by a blocky lignite (~130 cm).

The Cobham Lignite Bed at Cobham is underlain by the Upnor Formation, which, at a nearby site, is dated as latest Palaeocene by means of the occurrence of calcareous nannoplankton zone NP9 and magnetochron C25n in its lower part<sup>S10</sup>. The shallow-marine Woolwich Formation, which overlies the Cobham Lignite Bed at Cobham, contains the *Apectodinium* acme indicating that it is within the PETM<sup>S9,10</sup>. In addition, at Cobham a negative carbon isotope excursion (CIE) of ~ 1 ‰ is present near the top of the laminated lignite (54.4-55.3 cm) slightly below the middle clay layer, interpreted as being the negative CIE characteristic of the PETM<sup>S8-10</sup>. Here we used 7 samples from the lower laminated lignite below the inferred PETM CIE and thus of very latest Paleocene age.

### 1.3 Indian lignites

Lignites were collected from mines in several sites in the Rajasthan and Gujarat regions of western India (0-5 °N palaeolatitude). Paleogene-age subbituminous coals from the Meghalaya, Assam, and Nagaland regions of northeastern India were also analysed, but these lignites lacked GDGTs due to higher thermal maturity. All of these sections are associated with over- and/or underlying marine sediments, a characteristic consistent with deposition along the coastal margins of India<sup>S11-15</sup>. The elemental composition (relative concentration of C, H, O, N, and S) and TOC (total organic carbon) of the organic matter of Rajasthan and Gujarat lignites, in general, are suggestive of forest vegetation as the main source and peatification under topogenous conditions. This is further supported by the study of paleomires using petrography based information, using macerals as tools, which indicate deposition under tropical humid climatic conditions at a coastal setting with intermittent fluvial incursions<sup>S16-18</sup>.

Several lignites from the Kachchh Basin were analysed: one sample from the Matanomadh seam (present-day lat./long.: 23°30'05"N, 68°58'E) and two samples from the Panandhro seam (present lat./long.: 23°41'34"N, 68°46'24"E). The Naredi Formation, including these lignite seams, is largely constrained to the early to early middle Eocene on the basis of the age diagnostic foraminifera and pollen<sup>S11,19,20</sup>. Abundant dinoflagellate cysts in associated shales and mudstones and pollen

dominated by mangrove (*Nypa*) imply an occasional marine influence in a near-shore environment<sup>S20</sup>.

In addition, 3 lignite samples from the Khadsaliya Clays of the Saurashtra Basin (present lat./long. 21°39'32"N, 72°12'08"E) were analysed. These lignites are considered early Eocene on the basis of pollen and fungal remains<sup>S21,22</sup>. The Khadsaliya Clays comprise gray to greenish-gray clays, carbonaceous clay, and lignite deposited in a woody swamp<sup>S23</sup>.

Lastly, 3 lignite samples from the Palana Formation lignites were analyzed; one from the Barsingsar seam, Bikaner basin (present lat./long. 27.84°01N, 73.20°04E); and two from Kasnau Matasukh seam, Nagaur Basin (present lat./long.: 27°06'25"N, 74°04'30"E). The age of the Palana Formation is not well constrained. The Palana Formation was initially assigned to the Eocene on the basis of correlation with lignites in Pakistan<sup>S24</sup> and broad age constraints derived from pollen<sup>S25,26</sup>. However, planktonic foraminifera in the overlying Marh Formation have been suggested to be of late Paleocene-early Eocene age<sup>S27,28</sup>. In addition, the more recently described osteoglossid and lepisosteid fish are consistent with a Paleocene age for the Palana Formation<sup>S29</sup>. As such the Palana Formation is considered of late Paleocene age.

#### **1.4 Otaio River section lignites (New Zealand)**

The Paleocene to Eocene Broken River Formation overlain by the early Eocene Kauru Formation is exposed in the Otaio River section, near Otaio Gorge, eastern South Island, New Zealand. The Broken River Formation exposures include two lignite seams >1 m thick and several thinner lignite seams<sup>S30</sup>. Palynological analyses<sup>S31</sup> and unpublished data indicate that the lower portion of the Otaio River section spans the PETM and the rest of the Broken River Formation exposed in the Otaio River section belongs to the New Zealand stages Waipawan to Mangaorapan (56.0 Ma to 48.9 Ma)<sup>S32</sup>. In order to avoid possible overlap with the PETM, we used samples from only the upper lignites, i.e. early Eocene. The 6 samples analysed were taken from thin lignites separated by dark brown sandstones as well as from the c. 2m thick seam at the top of the Broken River Formation exposure in Otaio River. Palynological analyses indicate that the samples fall into the NZ MH1 pollen zone, except for the lowermost sample analysed here (OGp30) which is placed in the PM3b pollen zone.



## 2. Detection of *iso*GDGT-5 and -6 in peats and lignites

*Iso*GDGT-5 and -6 were identified based on 1) comparison of relative retention times (Fig. S2 and S3) with published data<sup>S33</sup>, 2) comparison of LC-MS chromatograms with those of a sample from Champagne pool, a thermal hot spring with a temperature of 75 °C and pH of 5.5 that contains *iso*GDGT-0 to -8<sup>S34</sup>, and an acid-hydrolysed extract of the extremophile *Thermoplasma acidophilum* (Matreya, catalog # 1303) (Fig. S4), which is known to produce *iso*GDGT-0 to -6, but not crenarchaeol<sup>S35</sup>, and 3) co-injection of a peat sample from Peru and the acid-hydrolysed extract of the extremophile *T. acidophilum* (Fig. S5).

## 3. Environmental controls on the *iso*GDGT distribution in modern peat

Decades of research, based on both culture experiments and natural archives such as marine sediments and thermal hot springs, have demonstrated that Archaea can alter the distribution of their *iso*GDGT membrane-spanning lipids in response to changes in environmental parameters such as temperature and pH<sup>S36-42</sup>. However, so far it is unknown whether the *iso*GDGT distribution in terrestrial settings such as peats varies according to environmental parameters. Below, we discuss the *iso*GDGT distribution in a wide range of modern peats to assess whether key-environmental parameters such as peat pH and mean air annual temperature have an impact on the *iso*GDGT pool in peats. The peat samples were obtained from a database as described in detail in Naafs et al.<sup>S43,44</sup>. In short, we analyzed >470 samples from 96 different peatlands from around the world for their GDGT distribution. The database consists of peats from a wide range of environments with a total span in mean annual air temperature (MAAT) from -8 to 27 °C and pH range from 3 to 8. pH data does not exist for all peats and *iso*GDGTs were below detection limit in a number of peat samples (predominantly in samples from the very top of peat).

### 3.1 pH dependence

In thermal hot springs, where *iso*GDGTs are produced by extremophiles, the *iso*GDGT distribution is influenced by environmental factors such as pH, with increasing cyclisation at lower pH and higher temperatures<sup>S34,41,45</sup>. It is largely unknown whether the *iso*GDGT distribution in mesophilic (terrestrial) settings is influenced by pH, although Xie et al.<sup>S46</sup> recently demonstrated that the *iso*GDGT

distributions of a number of Chinese and American mineral soils as well as enrichments of terrestrial *Thaumarchaeota* grown over a narrow pH range (6.5 to 8) were correlated with pH.

We found no significant correlation ( $R^2 < 0.2$ ) between the relative abundance of individual *iso*GDGTs with cyclopentane rings (both if crenarchaeol was included and when not) and pH (Fig. S6). The only *iso*GDGT that had a clear correlation ( $R^2 = 0.56$ ) with pH was *iso*GDGT-5.

We collected a range of samples from peatlands in the Peruvian Amazon. These tropical peats (MAAT  $\sim 26^\circ\text{C}$ ) are located less than 200 km apart, but span a pH range from 6.1 to 3.8. The peats with  $\text{pH} < 5.1$  contain *iso*GDGT-5, whereas those with a  $\text{pH} > 5.1$  do not (Fig. 2 of main manuscript). To explore this further, we compared the relative abundance of *iso*GDGT-5 relative to the other *iso*GDGTs with cyclopentane rings ( $5/(1+2+3+5)$ ) to the calcium concentration of individual samples. *Iso*GDGT-4 was excluded from this ratio due to the co-elution with the  $[\text{M}+\text{H}]^+ + 2$  ion of crenarchaeol that also gives  $m/z$  1294<sup>S47</sup>.

Calcium concentrations in peats are a good indicator of nutrient content and alkalinity (pH) in these peats<sup>S48</sup>. Calcium concentrations are low, typically less than 500 mg/kg dry peat, in nutrient-poor ombrotrophic bogs. River-influenced nutrient-rich minerotrophic peats with  $\text{pH} > 5$  are characterized by much higher calcium concentrations, up to 17,000 mg/kg dry peat<sup>S48,49</sup>. When we plot the  $5/(1+2+3+5)$  ratio against calcium concentration for individual peat samples (Fig. S7), it is clear that *iso*GDGT-5 is only present in samples with a low calcium content ( $< 2000$  mg/kg, mostly  $< 500$  mg/kg dry peat) and hence low pH. The CBT<sub>peat</sub>'-based pH calibration for peats has a relatively large error of  $\pm 0.8$  pH units and caution should be taken with applying CBT<sub>peat</sub>' to reconstruct absolute pH-values<sup>S43</sup>. Even so, the CBT<sub>peat</sub>' based pH values for these samples support the inferences derived from Ca ratios. *iso*GDGT-5 is only present in samples with CBT<sub>peat</sub>'-based  $\text{pH} < 5$  and predominantly in samples with CBT<sub>peat</sub>'-based  $\text{pH} < 4$ , as seen in the global dataset (Fig. 2 of the main manuscript).

In addition, a 750 cm long peat core from the Aucayacu peatland is characterized by a shift in peat forming environment. Sediments spanning 9 to 5 ka (below 400 cm) formed under minerotrophic conditions with high calcium concentrations (high pH), transitioning to low calcium concentrations (low pH) in the upper 400 cm spanning the late Holocene (last 5 kyr)<sup>S48,50</sup>. This transition occurred as

the peat deposit grew higher, out of river influence and into ombrotrophic conditions. *isoGDGT-5* is only present in the ombrotrophic (low pH), upper 400 cm of the core and absent in the underlying minerotrophic (high pH) peat (Fig. S8). Together, the modern surface samples and downcore results indicate a clear pH dependence controlling the abundance of *isoGDGT-5*.

$\text{TEX}_{86}^{\text{S38}}$  and the ring index (RI)<sup>S36</sup>, established indices that reflect the degree of cyclisation of *isoGDGTs*, did not correlate with pH (Fig. S9).

$$\text{TEX}_{86} = \frac{(\text{isoGDGT}_2 + \text{isoGDGT}_3 + \text{cren. isomer.})}{(\text{isoGDGT}_1 + \text{isoGDGT}_2 + \text{isoGDGT}_3 + \text{cren. isomer.})}$$

Ring index

$$= \frac{(\text{isoGDGT}_1 + 2 \times \text{isoGDGT}_2 + 3 \times \text{isoGDGT}_3 + 4 \times (\text{cren.} + \text{cren. isomer.}))}{(\text{isoGDGT}_0 + \text{isoGDGT}_1 + \text{isoGDGT}_2 + \text{isoGDGT}_3 + \text{cren.} + \text{cren. isomer.})}$$

### 3.2 Temperature dependence

Although the relationship differs between settings, both in culture experiments of hyperthermophiles and incubation experiments of mesophiles<sup>S36,40</sup> as well as natural archives such as marine<sup>S38</sup> and lake sediments<sup>S51</sup> and hot springs<sup>S34,41</sup> the degree of cyclization of *isoGDGTs*, reflected in RI and/or  $\text{TEX}_{86}$ , is positively correlated with growth temperature. So far it is largely unknown whether the cyclization of *isoGDGTs* in terrestrial settings is correlated to growth temperature, although there is some recent evidence that suggests that *isoGDGTs* in mineral soil altitude transects from Tanzania and China differ according to temperature<sup>S52,53</sup>.

Our results demonstrate that individual *isoGDGTs* with 0-3 cyclopentane rings have either no or weak ( $0.1 < R^2 < 0.2$ ) correlations with MAAT (Fig. S10). Also RI (with or without crenarchaeol) and  $\text{TEX}_{86}$  have no clear correlation with MAAT (Fig. S11). The lack of correlation between the distribution of *isoGDGTs* and MAAT is likely because the *isoGDGT* pool is derived from a mixture of GDGT-producing archaeal communities that thrive in peats. In regular marine sediments, the majority of GDGTs are derived from (planktonic) marine Thaumarchaeota that modify their membrane lipids depending on temperature, reflected in the  $\text{TEX}_{86}$  proxy. However the dominance of *isoGDGT-0* and low abundance of crenarchaeol in almost all peat samples, and resulting consistently low ring index, suggests a dominance of methanogenic Euryarchaeota. Consistent with this, if ring indices are calculated, excluding crenarchaeol, they remain poorly correlated to temperature and pH.

For *iso*GDGT-5 there is currently not enough data to construct a temperature calibration, especially due to the additional influence of pH on the relative abundance of *iso*GDGT-5 (see section 3.1). However, *iso*GDGT-5 is absent in ombrotrophic peats from the mid and high latitudes with MAAT < 12 °C. The highest relative abundance of *iso*GDGT-5 occurs in tropical peats accumulating under highest MAAT, indicating a temperature influence on the relative abundance of *iso*GDGT-5 (Fig. S10).

A combined pH/temperature control on the distribution of *iso*GDGT-5 is supported by four decades of research that reveal a pH and growth temperature dependence on *iso*GDGTs in cultures of acidohyperthermophilic Archaea<sup>S36</sup> and mesocosm experiments of marine Thaumarchaeota<sup>S40</sup>, as well as the observed correlation between the degree of cyclization and temperature and/or pH in natural environments such as hot springs<sup>S34</sup> and the open ocean<sup>S38</sup>. Amongst cultured organisms, Euryarchaeota belonging to the order Thermoplasmatales as well as Crenarchaeota of the orders Thermoproteales and Sulfolobales are the only known source organisms of *iso*GDGT-5 to -8<sup>S42</sup>; therefore, it is possible that (uncultured mesophilic) relatives of these specific orders are responsible for the presence of *iso*GDGT-5 to -7 in our modern ombrotrophic tropical peats and early Paleogene lignites.

#### 4. Environmental controls on the *br*GDGT distribution in modern peat

*br*GDGTs are membrane-spanning lipids produced by bacteria, likely acidobacteria<sup>S54-56</sup>. A decade of research has demonstrated that in mineral soils and lakes the degree of methylation of bacterial *br*GDGTs depends on temperature<sup>S57-60</sup>. We recently expanded this by developing a global peat-specific *br*GDGT temperature calibration that is based on the degree of methylation of *br*GDGTs, reflected in the MBT'<sub>5me</sub> index<sup>S57</sup>, in 470 samples from 96 different of modern peats: MAAT<sub>peat</sub><sup>S43</sup>. Importantly, the *br*GDGT data for this peat calibration dataset was generated using the latest HPLC-MS methods<sup>S61</sup> that separate the recently discovered 5- and 6-methyl *br*GDGTs<sup>S62</sup>.

$$\text{MBT}'_{5\text{me}} = \frac{(\text{Ia} + \text{Ib} + \text{Ic})}{(\text{Ia} + \text{Ib} + \text{Ic} + \text{IIa} + \text{IIb} + \text{IIc} + \text{IIIa})}$$

$$\text{MAAT}_{\text{peat}} (\text{°C}) = 52.18 \times \text{MBT}'_{5\text{me}} - 23.05 \quad (n = 96, \quad R^2 = 0.76,$$

$$\text{RMSE} = 4.7 \text{ °C})$$

In addition, the degree of cyclization of *br*GDGTs in mineral soils can be used to reconstruct pH<sup>S57,58</sup>. We recently demonstrated that also in peat the degree of cyclization of *br*GDGTs, expressed in the CBT<sub>peat</sub> index, is correlated with pH<sup>S43</sup>, although the correlation is weaker compared to that seen in mineral soils.

$$CBT_{\text{peat}} = \log \frac{(Ib + IIa' + IIb + IIb' + IIIa')}{(Ia + IIa + IIIa')}$$

$$pH = 2.49 \times CBT_{\text{peat}} + 8.07 \quad (n = 51, \quad R^2 = 0.58, \quad RMSE = 0.8)$$

As lignites are formed from compaction of peat under low burial pressure and temperatures, we apply this peat-specific calibration to reconstruct terrestrial temperatures during the early Paleogene. Inherent to this approach is the assumption that the relationship between MBT'<sub>5me</sub> and temperature was the same during the early Paleogene as at present.

GDGTs can be influenced by thermal maturation. Schouten et al.<sup>S42,63</sup> showed that *iso*- and *br*GDGTs are similarly influenced by thermal degradation as GDGTs disappear at hydrous pyrolysis temperatures > 260 °C. Consistent with these experiments, GDGTs appear to be absent in thermally mature coal<sup>S64</sup>. In addition, thermal maturation of GDGTs between ~220 and 260 °C was shown to influence their distribution, with a decrease in the degree of methylation and cyclization<sup>S42,63</sup>. Thus, thermal maturation can not explain the high temperatures we reconstruct for the early Paleogene using lignites as 1) lignites are formed at low burial temperatures (<100 °C) where GDGTs are not influenced, and 2) if thermal degradation would have influenced the *br*GDGTs in our lignites, this would have lowered MBT'<sub>5me</sub> and hence resulted in low MAAT<sub>peat</sub>.

## 5. GDGT distribution early Paleogene lignites

As explained in the previous section, we assume that the relationship observed in modern peat between MBT'<sub>5me</sub> and temperature<sup>S43</sup> was the same during the early Paleogene. This assumption is supported by the observation that the broader GDGT distribution in our lignites, of which the majority formed between 45 and 60 degrees latitude during the early Paleogene, is very similar to modern-day distribution of GDGTs in tropical peats. The lignite and tropical modern-day peat are characterized by a high abundance of *iso*GDGTs with cyclopentane rings (including *iso*GDGT-5), H-*iso*GDGTs<sup>S44</sup> (characterized by a covalent bond between the two alkyl chains<sup>S65</sup>), and dominance of *br*GDGT-Ia over the other *br*GDGTs. On the other hand, the

GDGT distribution in our lignites looks different compared to a modern-day mid-latitude peat (Fig. S12). Modern-day mid-latitude peats lack significant amounts of *iso*GDGTs with cyclopentane rings, do not contain *iso*GDGT-5 or H-*iso*GDGTs, and penta- and hexamethylated *br*GDGT are abundant.

Sinninghe Damsté<sup>S66</sup> recently used a ternary plot of the *br*GDGT distribution in marine sediments and argued that samples that plot off the *br*GDGT distribution seen in the modern mineral soil database contain a contribution of *in situ* *br*GDGT production and do not exclusively contain mineral soil-derived terrestrial *br*GDGTs. Following this approach, if the GDGT distribution of our early Paleogene lignites was not produced in peats, the lignite data should plot outside of distribution of *br*GDGTs in the modern peat database. However, when we compare the *br*GDGT distribution in our early Paleogene lignites to that of modern peats<sup>S43</sup> using ternary plots (Fig. S13), it is clear that the *br*GDGT distribution of early Paleogene lignites looks very similar to that in modern peatlands. We then extended this approach by comparing the *iso*GDGT distribution in our early Paleogene lignites with that seen in modern peats and marine core-top sediments (Fig. S14). The *iso*GDGT distribution in our early Paleogene lignites looks very similar to that seen in modern-day peats with a very low proportion of crenarchaeol and looks very different from the *iso*GDGT distribution of for example marine sediments<sup>S67</sup>. These results highlight that not only MBT'<sub>5me</sub> (and hence MAAT<sub>peat</sub>) and the abundance of *iso*GDGT-5 in our early Paleogene lignites are similar to modern (tropical) peats, but that the broader GDGT distribution of our early Paleogene lignites is comparable to a modern-day (tropical) peat.

The only difference is the abundance of *iso*GDGT-5 encountered in the Indian lignites, which is higher than found in any modern peat, even in modern tropical peats (MAAT ~ 26.5 °C) with pH ~ 3. As pH of 3 is the most acidic peat environment known, the higher abundance of *iso*GDGT-5 found in the Indian lignites is at least partly related to temperatures higher than MAAT > 26.5 °C, inline with our MAAT<sub>peat</sub> temperature estimates. In addition, it is unlikely that the high abundance of *iso*GDGT-5 in the Indian lignites (compared to the mid-latitude lignites) is the result of a much lower pH. For example there is independent evidence that at least some of the mid-latitude lignites were formed in ombrotrophic (low pH) *Sphagnum* peats<sup>S4</sup> and CBT<sub>peat</sub>' is similar for all lignites.

## 6. Calculation of paleolatitudes

To be consistent the Ypresian paleolatitudes for all published terrestrial (and marine) sites as well as the lignites were (re)calculated using the models explained in<sup>S68</sup>. These paleolatitudes might differ slightly from those reported in the original publications. The uncertainty in the paleolatitude calculations for each site is not known, but can be up to several degrees paleolatitude.

## **7. Compilation of published early Paleogene terrestrial temperatures**

We compiled terrestrial temperature data based on a range of proxy methods as plotted in figure 1. The majority of data is obtained using leaf physiognomy from the early Paleogene (late Paleocene and early Eocene) and derived mainly from the Huber and Caballero<sup>S69</sup> and Yang et al.<sup>S70</sup> compilations (**see data file**). There are different leaf physiognomy methods and we grouped them into three groups 1) data obtained using the Kowalski and Ditcher (K&D) leaf margin analysis calibration<sup>S71</sup>, 2) data obtained using Climate Leaf Analysis Multivariate Program (CLAMP), and 3) other leaf physiognomy data (e.g. using alternative leaf margin analysis calibrations<sup>S72</sup>). Estimates based on nearest living relatives data from plants (e.g. coexistence approach, bioclimatic analysis, etc) were omitted from figure 1 and 3 because of their reliance on correct identification of the nearest living relative. For comparison, figures S15 and S16 include this nearest living relative temperature data. In addition, we omitted a number of data points from the various compilations either because the data was confirmed to be middle Eocene in age (Axel Heidelberg, Geiseltal, Puryear-Buchanan, Kisinger Lakes, Chermurnaut Bay, Fossil Hill Flora - King George Island, and James Ross Basin), represented the PETM (Dragon Glacier - King George Island, Hubble Bubble – Bighorn Basin), the age of the data was poorly constrained (Mahenge and Raichikha), or because the altitude correction applied was uncertain (China Gulch, Camanche Bridge, Pentz, Cherokee Site 1, Fiona Hill, Council Hill, Iowa Hill, You Bet 2, Chalk Bluffs – E., Scotts Flat, Gold Bug, Hidden Gold Camp, Woolsey Flat, Mountain Boy, and Pine Grove 1). From Yang et al.<sup>S70</sup> we used the gridded data adjusted.

Where available we show MAAT obtained using different calibrations to show the full uncertainty regarding leaf physiognomy based MAATs. For Climate Leaf Analysis Multivariate Program (CLAMP) data<sup>S70</sup> we use an uncertainty of  $\pm 2$  °C ([http://clamp.ibcas.ac.cn/CLAMP\\_Uncertainties.html](http://clamp.ibcas.ac.cn/CLAMP_Uncertainties.html)). We want to highlight that use of the Kowalski and Ditcher (K&D) calibration used in Huber and Caballero<sup>S69</sup> often



does lead to higher MAAT estimates compared to other calibrations (e.g. CLAMP), but it is based on a very limited dataset.

All the previously published MBT/CBT-based mineral soil-derived MAAT<sup>S31,73-77</sup>, based on the distribution of *br*GDGTs in (proximal) marine sediments, were revised using the updated MBT'/CBT calibration<sup>S78</sup>. The errors shown in figure 1 for the MBT'/CBT based data were obtained by adding the 5 °C calibration error of the MBT'/CBT calibration<sup>S78</sup> to the one standard deviation of the MBT'/CBT data for each site. For MAAT<sub>peat</sub> the error bars were calculated the same way, but using a calibration error of 4.7 °C<sup>S43</sup>. Only data spanning the late Paleocene and early Eocene (57-48 Myr) was used ([see data file](#)). Where the PETM was recognized; data from the PETM was excluded.

We also included temperature data from early Paleogene paleosols from Argentina<sup>S79</sup> and the USA<sup>S80</sup> as well as early Paleogene  $\delta^{18}\text{O}$ -based terrestrial temperatures from mammalian tooth enamel and fish (gar) scales, all from the Northern Hemisphere<sup>S81,82</sup>.

## 8. Compilation of published early Paleogene sea surface temperatures

To compare our early Paleogene terrestrial temperature data with sea surface temperature (SST) data, we compiled all available published data based on the organic geochemical TEX<sub>86</sub> palaeothermometer as well as calcite-based SSTs using Mg/Ca and  $\delta^{18}\text{O}$  of pristine planktonic foraminifera and clumped isotopes ([see data file](#)). TEX<sub>86</sub>-based SSTs were calculated using the BAYSPAR deep time analog approach<sup>S67,83</sup>. Error bars on TEX<sub>86</sub>-based SST in figure 1 represent the 1 $\sigma$  confidence interval. For the calcite-based proxies the errors were calculated by combining the calibration error and the one standard deviation of the data for each site under different assumptions of early Paleogene seawater composition;  $-0.64 < \delta^{18}\text{O}_{\text{sw}}$  (VSMOW)  $< -0.21$ <sup>S84</sup> and  $1.5 < (\text{Mg}/\text{Ca})_{\text{sw}} < 5$ <sup>S85</sup>. Only data spanning the late Paleocene and early Eocene (57-48 Myr) was used ([see data file](#)). Where the PETM was recognized SST data from the PETM was excluded.

## 9. Data model comparison

The model-data comparison shown in Figure 3 is carried out using identical methods to those outlined in Lunt et al.<sup>S84</sup>. In brief, the early Paleogene zonal mean near-surface (~2m) continental air temperature is calculated for each of 7 models using



different  $p\text{CO}_2$  concentrations; 2x $\text{CO}_2$  ECHAM5<sup>S86</sup>, 2x $\text{CO}_2$  FAMOUS<sup>S87</sup>, 4x $\text{CO}_2$  GISS<sup>S88</sup>, 5x $\text{CO}_2$  CCSM3\_K<sup>S89</sup>, 6x $\text{CO}_2$  HadCM3L<sup>S90</sup>, 16x $\text{CO}_2$  CCSM3\_W<sup>S91</sup> and 16x $\text{CO}_2$  CCSM3\_H<sup>S69</sup>. The prescribed Eocene paleogeography also varies across the simulations as shown in the relevant references cited above.

An equivalent temperature (but global rather than continental) from an equivalent preindustrial simulation from each model is also calculated, and the difference, early Paleogene minus pre-industrial, is shown as coloured lines in Figure 3. In the nomenclature of Lunt et al.<sup>S84</sup>, this is  $[\overline{LAT_{ep}} - \overline{GAT_p}]$ . On top of these modelled zonal mean anomalies, our compilation of proxy early Paleogene terrestrial temperatures is plotted, including our new MAAT<sub>peat</sub> estimates, and including published estimates of uncertainties. These proxy temperatures are plotted as anomalies relative to the zonal mean of observed modern global (not exclusively terrestrial) near-surface air temperatures, (NCEP<sup>S92</sup>), for the period 1981–2010. As such, the proxy data represent temperature anomalies at a single site, whereas the modelled results are zonal means.

### Supplementary references

- S1 Robson, B. E. *et al.* Early Paleogene wildfires in peat-forming environments at Schöningen, Germany, *Palaeogeogr. Palaeoclimatol. Palaeoecol.* **437**, 53-62, (2015).
- S2 Inglis, G. N. *et al.* Mid-latitude continental temperatures through the early Eocene in western Europe, *Earth Plant. Sc. Lett.* **460**, 86-96, (2017).
- S3 Riegel, W., Wilde, V. & Lenz, O. K. The early Eocene of Schöningen (N-Germany) - an interim report, *Aust. J. Earth Sci.* **105**, 88-109, (2012).
- S4 Inglis, G. N. *et al.* Ecological and biogeochemical change in an early Paleogene peat-forming environment: Linking biomarkers and palynology, *Palaeogeogr. Palaeoclimatol. Palaeoecol.* **438**, 245-255, (2015).
- S5 Ahrendt, H., Köthe, A., Lietzow, A., Marhein, D. & Ritzkowski, S. Lithostratigraphy, biostratigraphy and radiometric dating of the Early Eocene at Helmstedt (Lower Saxony), *Z. Dtsch. Geol. Ges.* **146**, 450-457, (1995).
- S6 Crouch, E. M. *et al.* The *Apectodinium* acme and terrestrial discharge during the Paleocene–Eocene thermal maximum: new palynological, geochemical and calcareous nannoplankton observations at Tawanui, New Zealand, *Palaeogeogr. Palaeoclimatol. Palaeoecol.* **194**, 387-403, (2003).
- S7 Sluijs, A. *et al.* Environmental precursors to rapid light carbon injection at the Palaeocene/Eocene boundary, *Nature* **450**, 1218-1221, (2007).
- S8 Pancost, R. D. *et al.* Increased terrestrial methane cycling at the Palaeocene-Eocene thermal maximum, *Nature* **449**, 332-335, (2007).

- 409 S9 Collinson, M. E., Hooker, J. J. & Gröcke, D. R. in *Causes and Consequences of*  
410 *Globally Warm Climates in the Early Paleogene* Vol. 369 (eds Scott L. Wing,  
411 P.D. Gingerich, B. Schmitz, & B. Thomas) 333-349 (Geological Society of  
412 America, 2003).
- 413 S10 Collinson, M. E. *et al.* Palynological evidence of vegetation dynamics in  
414 response to palaeoenvironmental change across the onset of the  
415 Paleocene - Eocene Thermal Maximum at Cobham, Southern England,  
416 *Grana* **48**, 38-66, (2009).
- 417 S11 Biswas, S. K. Tertiary stratigraphy of Kutch, *J. Palaeontol. Soc. Ind.* **37**, 1-  
418 29, (1992).
- 419 S12 Sahni, N., Rose, K. D., Singh, L. & Smith, T. Temporal constraints and  
420 depositional paleoenvironments of the Vastan lignite sequences, Gujarat:  
421 Analogy for Cambay shale Hydrocarbon source rock, *Indian J. Petrol. Geol.*  
422 **15**, 1-20, (2006).
- 423 S13 McCann, T. Chenier plain sedimentation in the Palaeogene-age lignite-rich  
424 successions of the Surat area, Gujarat, western India, *Z. Dtsch. Geol. Ges.*  
425 **161**, 335-351, (2010).
- 426 S14 Singh, P. K. *et al.* Petrological and Geochemical Investigations of Rajpardi  
427 Lignite Deposit, Gujarat, India, *Energ. Explor. Exploit.* **30**, 131-151, (2012).
- 428 S15 Singh, A. K., Singh, M. P. & Singh, P. K. Petrological investigations of  
429 Oligocene coals from foreland basin of northeast India, *Energ. Explor.*  
430 *Exploit.* **31**, 909-936, (2013).
- 431 S16 Singh, P. K., Singh, M. P. & Singh, A. K. Petro-chemical characterization and  
432 evolution of Vastan Lignite, Gujarat, India, *Int. J. Coal Geol.* **82**, 1-16,  
433 (2010).
- 434 S17 Singh, P. K., Rajak, P. K., Singh, M. P., Singh, V. K. & Naik, A. S. Geochemistry  
435 of Kasnau-Matasukh lignites, Nagaur basin, Rajasthan (India), *Inter. J. Coal*  
436 *Sc. Tech.* **3**, 104-122, (2016).
- 437 S18 Singh, P. K. *et al.* Peat swamps at Giral lignite field of Barmer basin,  
438 Rajasthan, Western India: Understanding the Evolution through  
439 Petrological Modelling, *Inter. J. Coal Sc. Tech.* **3**, 148-164, (2016).
- 440 S19 Dutta, S. *et al.* Petrology, palynology and organic geochemistry of Eocene  
441 lignite of Matanomadh, Kutch Basin, western India: Implications to  
442 depositional environment and hydrocarbon source potential, *Int. J. Coal*  
443 *Geol.* **85**, 91-102, (2011).
- 444 S20 Mathews, R. P., Tripathi, S. M., Banerjee, S. & Dutta, S. Palynology,  
445 palaeoecology and palaeodepositional environment of Eocene lignites and  
446 associated sediments from Matanomadh mine, Kutch Basin, western  
447 India, *J. Geol. Soc. India* **82**, 236-248, (2013).
- 448 S21 Samant, B. Palynostratigraphy and age of the Bhavnagar lignite, Gujarat,  
449 India, *Palaeobotanist* **49**, 101-108, (2000).
- 450 S22 Samant, B. Fungal remains from the Bhavnagar lignite, Gujarat, India,  
451 *Geophytology* **28**, 11-18, (2000).
- 452 S23 Thakur, O. P., Singh, A. & Singh, B. D. Petrographic characterization of  
453 Khadsaliya lignites, Bhavnagar district, Gujarat, *J. Geol. Soc. India* **76**, 40-46,  
454 (2010).
- 455 S24 La Touche, T. D. Report on the Occurrence of coal at Palana village in  
456 Bikaner State, *Record of the Geological Society of India* **30**, (1897).

- 457 S25 Rao, S. R. N. & Vimal, K. P. Tertiary pollen from lignite from Palana  
458 (Eocene) Bikaner, *Proc. Nat. Instit. Sci. India* **18**, 595-601, (1952).
- 459 S26 Tripathi, R. P., Si Sodha, M. S., Srivastava, K. L. & Sharma, B. D. in *Geological*  
460 *evolution of northwestern India* (ed B.S. Paliwal) 118–128 (Scientific  
461 Publishers, 1999).
- 462 S27 Singh, S. N. Planktonic foraminifera in the Eocene stratigraphy of  
463 Rajasthan, India, *roceedings of the 2nd International Conference on*  
464 *Planktonic Microfossils, Rome* **2**, 1169–1181, (1971).
- 465 S28 Tripathi, S. K. M., Mathur, S. C., Nama, S. L. & Srivastava, D. in *Palaeobotany*  
466 *to modern botany* (ed P.C. Trivedi) 49–56 (Pointer Publishers, 2006).
- 467 S29 Kumar, K., Rana, R. S. & Paliwal, B. S. Osteoglossid and lepisosteid fish  
468 remains from the Paleocene Palana formation, Rajasthan, India,  
469 *Palaeontology* **48**, 1187–1209, (2005).
- 470 S30 Field, B. D., Browne, G. H. & Davy, B. W. Cretaceous and Cenozoic  
471 sedimentary basins and geological evolution of the Canterbury region,  
472 South Island, New Zealand, (New Zealand Geological Survey, 1989).
- 473 S31 Pancost, R. D. *et al.* Early Paleogene evolution of terrestrial climate in the  
474 SW Pacific, Southern New Zealand, *Geochem. Geophys. Geosyst.* **14**, 5413-  
475 5429, (2013).
- 476 S32 Raine, J. I. *et al.* New Zealand Geological Timescale NZGT 2015/1, *New*  
477 *Zeal. J. Geol. Geop.* **58**, 398-403, (2015).
- 478 S33 Pearson, A. & Rusch, D. B. Distribution of microbial terpenoid lipid  
479 cyclases in the global ocean metagenome, *ISME J.* **3**, 352-363, (2008).
- 480 S34 Kaur, G., Mountain, B., Stott, M., Hopmans, E. & Pancost, R. Temperature  
481 and pH control on lipid composition of silica sinters from diverse hot  
482 springs in the Taupo Volcanic Zone, New Zealand, *Extremophiles* **19**, 327-  
483 344, (2015).
- 484 S35 Shimada, H., Nemoto, N., Shida, Y., Oshima, T. & Yamagishi, A. Effects of pH  
485 and Temperature on the Composition of Polar Lipids in *Thermoplasma*  
486 *acidophilum* HO-62, *J. Bacteriol.* **190**, 5404-5411, (2008).
- 487 S36 De Rosa, M., Esposito, E., Gambacorta, A., Nicolaus, B. & Bu'Lock, J. D.  
488 Effects of temperature on ether lipid composition of *Caldariella*  
489 *acidophila*, *Phytochemistry* **19**, 827-831, (1980).
- 490 S37 De Rosa, M. & Gambacorta, A. The lipids of archaebacteria, *Prog. Lipid Res.*  
491 **27**, 153-175, (1988).
- 492 S38 Schouten, S., Hopmans, E. C., Schefuss, E. & Sinninghe Damsté, J. S.  
493 Distributional variations in marine crenarchaeotal membrane lipids: a  
494 new tool for reconstructing ancient sea water temperatures?, *Earth Plant.*  
495 *Sc. Lett.* **204**, 265-274, (2002).
- 496 S39 Elling, F. J., Könneke, M., Mußmann, M., Greve, A. & Hinrichs, K.-U.  
497 Influence of temperature, pH, and salinity on membrane lipid composition  
498 and TEX<sub>86</sub> of marine planktonic thaumarchaeal isolates, *Geochim.*  
499 *Cosmochim. Acta* **171**, 238-255, (2015).
- 500 S40 Schouten, S., Forster, A., Panoto, F. E. & Sinninghe Damsté, J. S. Towards  
501 calibration of the TEX<sub>86</sub> palaeothermometer for tropical sea surface  
502 temperatures in ancient greenhouse worlds, *Org. Geochem.* **38**, 1537-  
503 1546, (2007).

504 S41 Pearson, A. *et al.* Factors Controlling the Distribution of Archaeal  
 505 Tetraethers in Terrestrial Hot Springs, *Appl. Environ. Microbiol.* **74**, 3523-  
 506 3532, (2008).  
 507 S42 Schouten, S., Hopmans, E. C. & Sinninghe Damsté, J. S. The organic  
 508 geochemistry of glycerol dialkyl glycerol tetraether lipids: A review, *Org.*  
 509 *Geochem.* **54**, 19-61, (2013).  
 510 S43 Naafs, B. D. A. *et al.* Introducing global peat-specific temperature and pH  
 511 calibrations based on brGDGT bacterial lipids, *Geochim. Cosmochim. Acta*  
 512 **208**, 285-301, (2017).  
 513 S44 Naafs, B. D. A., McCormick, D., Inglis, G. N. & Pancost, R. D. Archaeal and  
 514 bacterial H-GDGTs are abundant in peat and their relative abundance is  
 515 positively correlated with temperature, *Geochim. Cosmochim. Acta* **227**,  
 516 156-170, (2018).  
 517 S45 Wu, W. *et al.* Impacts of temperature and pH on the distribution of  
 518 archaeal lipids in Yunnan hot springs, China, *Front. Microbiol.* **4**, 312,  
 519 (2013).  
 520 S46 Xie, W., Zhang, C. & Ma, C. Temporal variation in community structure and  
 521 lipid composition of Thaumarchaeota from subtropical soil: Insight into  
 522 proposing a new soil pH proxy, *Org. Geochem.* **83-84**, 54-64, (2015).  
 523 S47 Weijers, J. W. H., Schouten, S., van der Linden, M., van Geel, B. & Sinninghe  
 524 Damsté, J. S. Water table related variations in the abundance of intact  
 525 archaeal membrane lipids in a Swedish peat bog, *FEMS Microbiol. Lett.*  
 526 **239**, 51-56, (2004).  
 527 S48 Låhteenoja, O. & Page, S. High diversity of tropical peatland ecosystem  
 528 types in the Pastaza-Marañón basin, Peruvian Amazonia, *J. Geophys. Res.*  
 529 *Biogeosci.* **116**, (2011).  
 530 S49 Låhteenoja, O., Ruokolainen, K., Schulman, L. & Alvarez, J. Amazonian  
 531 floodplains harbour minerotrophic and ombrotrophic peatlands, *Catena*  
 532 **79**, 140-145, (2009).  
 533 S50 Låhteenoja, O. *et al.* The large Amazonian peatland carbon sink in the  
 534 subsiding Pastaza-Marañón foreland basin, Peru, *Global Change Biol.* **18**,  
 535 164-178, (2012).  
 536 S51 Powers, L. *et al.* Applicability and calibration of the TEX<sub>86</sub>  
 537 paleothermometer in lakes, *Org. Geochem.* **41**, 404-413, (2010).  
 538 S52 Coffinet, S., Huguet, A., Williamson, D., Fosse, C. & Derenne, S. Potential of  
 539 GDGTs as a temperature proxy along an altitudinal transect at Mount  
 540 Rungwe (Tanzania), *Org. Geochem.* **68**, 82-89, (2014).  
 541 S53 Yang, H., Pancost, R. D., Jia, C. & Xie, S. The Response of Archaeal  
 542 Tetraether Membrane Lipids in Surface Soils to Temperature: A Potential  
 543 Paleothermometer in Paleosols, *Geomicrobiol. J.* **33**, 98-109, (2016).  
 544 S54 Weijers, J. W. H. *et al.* Membrane lipids of mesophilic anaerobic bacteria  
 545 thriving in peats have typical archaeal traits, *Environ. Microbiol.* **8**, 648-  
 546 657, (2006).  
 547 S55 Sinninghe Damsté, J. S. *et al.* 13,16-Dimethyl Octacosanedioic Acid (*iso*-  
 548 Diabolic Acid), a Common Membrane-Spanning Lipid of *Acidobacteria*  
 549 Subdivisions 1 and 3, *Appl. Environ. Microb.* **77**, 4147-4154, (2011).  
 550 S56 Sinninghe Damsté, J. S. *et al.* Ether- and Ester-Bound *iso*-Diabolic Acid and  
 551 Other Lipids in Members of *Acidobacteria* Subdivision 4, *Appl. Environ.*  
 552 *Microb.* **80**, 5207-5218, (2014).

553 S57 De Jonge, C. *et al.* Occurrence and abundance of 6-methyl branched  
554 glycerol dialkyl glycerol tetraethers in soils: implications for  
555 palaeoclimate reconstruction, *Geochim. Cosmochim. Acta* **141**, 97-112,  
556 (2014).

557 S58 Weijers, J. W. H., Schouten, S., van den Donker, J. C., Hopmans, E. C. &  
558 Sinninghe Damsté, J. S. Environmental controls on bacterial tetraether  
559 membrane lipid distribution in soils, *Geochim. Cosmochim. Acta* **71**, 703-  
560 713, (2007).

561 S59 Naafs, B. D. A., Gallego-Sala, A. V., Inglis, G. N. & Pancost, R. D. Refining the  
562 global branched glycerol dialkyl glycerol tetraether (brGDGT) soil  
563 temperature calibration, *Org. Geochem.* **106**, 48-56, (2017).

564 S60 Loomis, S. E., Russell, J. M., Ladd, B., Street-Perrott, F. A. & Sinninghe  
565 Damsté, J. S. Calibration and application of the branched GDGT  
566 temperature proxy on East African lake sediments, *Earth Planet. Sc. Lett.*  
567 **357-358**, 277-288, (2012).

568 S61 Hopmans, E. C., Schouten, S. & Sinninghe Damsté, J. S. The effect of  
569 improved chromatography on GDGT-based palaeoproxies, *Org. Geochem.*  
570 **93**, 1-6, (2016).

571 S62 De Jonge, C. *et al.* Identification of novel penta- and hexamethylated  
572 branched glycerol dialkyl glycerol tetraethers in peat using HPLC-MS<sup>2</sup>,  
573 GC-MS and GC-SMB-MS, *Org. Geochem.* **54**, 78-82, (2013).

574 S63 Schouten, S., Hopmans, E. C. & Sinninghe Damsté, J. S. The effect of  
575 maturity and depositional redox conditions on archaeal tetraether lipid  
576 palaeothermometry, *Org. Geochem.* **35**, 567-571, (2004).

577 S64 Weijers, J. W. H., Steinmann, P., Hopmans, E. C., Schouten, S. & Sinninghe  
578 Damsté, J. S. Bacterial tetraether membrane lipids in peat and coal:  
579 Testing the MBT-CBT temperature proxy for climate reconstruction, *Org.*  
580 *Geochem.* **42**, 477-486, (2011).

581 S65 Morii, H. *et al.* A novel ether core lipid with H-shaped C<sub>80</sub>-isoprenoid  
582 hydrocarbon chain from the hyperthermophilic methanogen  
583 *Methanothermus fervidus*, *BBA-Lipid Lipid Met.* **1390**, 339-345, (1998).

584 S66 Sinninghe Damsté, J. S. Spatial heterogeneity of sources of branched  
585 tetraethers in shelf systems: The geochemistry of tetraethers in the Berau  
586 River delta (Kalimantan, Indonesia), *Geochim. Cosmochim. Acta* **186**, 13-  
587 31, (2016).

588 S67 Tierney, J. E. & Tingley, M. P. A TEX<sub>86</sub> surface sediment database and  
589 extended Bayesian calibration, *Sci. Data* **2**, 150029, (2015).

590 S68 Lunt, D. J. *et al.* Palaeogeographic controls on climate and proxy  
591 interpretation, *Clim. Past* **12**, 1181-1198, (2016).

592 S69 Huber, M. & Caballero, R. The early Eocene equable climate problem  
593 revisited, *Clim. Past* **7**, 603-633, (2011).

594 S70 Yang, J., Spicer, R. A., Spicer, T. E. V. & Li, C.-S. 'CLAMP Online': a new web-  
595 based palaeoclimate tool and its application to the terrestrial Paleogene  
596 and Neogene of North America, *Palaeobiodivers. palaeoenviron.* **91**, 163-  
597 183, (2011).

598 S71 Kowalski, E. A. & Dilcher, D. L. Warmer paleotemperatures for terrestrial  
599 ecosystems, *Proc. Natl. Acad. Sci.* **100**, 167-170, (2003).

600 S72 Peppe, D. J. *et al.* Sensitivity of leaf size and shape to climate: global  
 601 patterns and paleoclimatic applications, *New Phytol.* **190**, 724-739,  
 602 (2011).  
 603 S73 Weijers, J. W. H., Schouten, S., Sluijs, A., Brinkhuis, H. & Sinninghe Damsté,  
 604 J. S. Warm arctic continents during the Palaeocene–Eocene thermal  
 605 maximum, *Earth Planet. Sc. Lett.* **261**, 230-238, (2007).  
 606 S74 Sluijs, A. *et al.* Warming, euxinia and sea level rise during the Paleocene–  
 607 Eocene Thermal Maximum on the Gulf Coastal Plain: implications for  
 608 ocean oxygenation and nutrient cycling, *Clim. Past* **10**, 1421-1439, (2014).  
 609 S75 Keating-Bitonti, C. R., Ivany, L. C., Affek, H. P., Douglas, P. & Samson, S. D.  
 610 Warm, not super-hot, temperatures in the early Eocene subtropics,  
 611 *Geology* **39**, 771-774, (2011).  
 612 S76 Bijl, P. K. *et al.* Eocene cooling linked to early flow across the Tasmanian  
 613 Gateway, *P. Natl. Acad. Sci. USA* **110**, 9645-9650, (2013).  
 614 S77 Schoon, P. L., Heilmann-Clausen, C., Schultz, B. P., Sinninghe Damsté, J. S. &  
 615 Schouten, S. Warming and environmental changes in the eastern North  
 616 Sea Basin during the Palaeocene–Eocene Thermal Maximum as revealed  
 617 by biomarker lipids, *Org. Geochem.* **78**, 79-88, (2015).  
 618 S78 Peterse, F. *et al.* Revised calibration of the MBT–CBT paleotemperature  
 619 proxy based on branched tetraether membrane lipids in surface soils,  
 620 *Geochim. Cosmochim. Acta* **96**, 215-229, (2012).  
 621 S79 Hyland, E. G., Sheldon, N. D. & Cotton, J. M. Constraining the early Eocene  
 622 climatic optimum: A terrestrial interhemispheric comparison, *Geol. Soc.*  
 623 *Am. Bull.* **129**, 244-252, (2017).  
 624 S80 Hyland, E., Sheldon, N. D. & Fan, M. Terrestrial paleoenvironmental  
 625 reconstructions indicate transient peak warming during the early Eocene  
 626 climatic optimum, *Geol. Soc. Am. Bull.* **125**, 1338-1348, (2013).  
 627 S81 Hyland, E. G. & Sheldon, N. D. Coupled CO<sub>2</sub>-climate response during the  
 628 Early Eocene Climatic Optimum, **369**, 125-135, (2013).  
 629 S82 Fricke, H. C. & Wing, S. L. Oxygen isotope and paleobotanical estimates of  
 630 temperature and  $\delta^{18}\text{O}$ -latitude gradients over North America during the  
 631 early Eocene, *Am. J. Sci.* **304**, 612-635, (2004).  
 632 S83 Tierney, J. E. & Tingley, M. P. A Bayesian, spatially-varying calibration  
 633 model for the TEX<sub>86</sub> proxy, *Geochim. Cosmochim. Acta* **127**, 83-106,  
 634 (2014).  
 635 S84 Lunt, D. J. *et al.* A model–data comparison for a multi-model ensemble of  
 636 early Eocene atmosphere–ocean simulations: EoMIP, *Clim. Past* **8**, 1717-  
 637 1736, (2012).  
 638 S85 Higgins, J. A. & Schrag, D. P. The Mg isotopic composition of Cenozoic  
 639 seawater – evidence for a link between Mg-clays, seawater Mg/Ca, and  
 640 climate, *Earth Planet. Sc. Lett.* **416**, 73-81, (2015).  
 641 S86 Heinemann, M., Jungclaus, J. H. & Marotzke, J. Warm Paleocene/Eocene  
 642 climate as simulated in ECHAM5/MPI-OM, *Clim. Past* **5**, 785-802, (2009).  
 643 S87 Sagoo, N., Valdes, P., Flecker, R. & Gregoire, L. J. The Early Eocene equable  
 644 climate problem: can perturbations of climate model parameters identify  
 645 possible solutions?, *Philos. T. Roy. Soc. A* **371**, 0123, (2013).  
 646 S88 Roberts, C. D., LeGrande, A. N. & Tripathi, A. K. Climate sensitivity to Arctic  
 647 seaway restriction during the early Paleogene, *Earth Plant. Sc. Lett.* **286**,  
 648 576-585, (2009).

- S89 Kiehl, J. T. & Shields, C. A. Sensitivity of the Palaeocene–Eocene Thermal  
Maximum climate to cloud properties, *Philos. T. Roy. Soc. A* **371**, 0093,  
(2013).
- S90 Lunt, D. J. *et al.* CO<sub>2</sub>-driven ocean circulation changes as an amplifier of  
Paleocene-Eocene thermal maximum hydrate destabilization, *Geology* **38**,  
875-878, (2010).
- S91 Winguth, A., Shellito, C., Shields, C. & Winguth, C. Climate Response at the  
Paleocene–Eocene Thermal Maximum to Greenhouse Gas Forcing—A  
Model Study with CCSM3, *J. Climate* **23**, 2562-2584, (2009).
- S92 Kalnay, E. *et al.* The NCEP/NCAR 40-Year Reanalysis Project, *Bull. Am.*  
*Meteorol. Soc.* **77**, 437-471, (1996).

# **Supplementary figure captions**

Figure S1; Present-day location of the lignites used in this study.

Figure S2; HPLC-APCI-MS base peak chromatogram (top) and mass chromatograms  
of a tropical peat sample from Peru (the Aucayacu peatland, 330 cm depth). Numbers  
indicate number of cyclopentane moieties in the *iso*GDGTs, while roman numbers  
highlight the different *br*GDGTs. Cren = crenarchaeol and reg.iso= crenarchaeol  
regioisomer. In H-*iso*GDGTs the two biphytane chains are covalently bound by a  
carbon-carbon bond<sup>S65</sup>.

Figure S3; HPLC-APCI-MS base peak chromatogram (top) and mass chromatograms  
of an early Paleogene lignite sample from Cobham (CL70, 11.95 cm). Numbers  
indicate number of cyclopentane moieties in the *iso*GDGTs, while roman numbers  
highlight the different *br*GDGTs. Cren = crenarchaeol and reg.iso= crenarchaeol  
regioisomer. In H-GDGTs the two biphytane chains are covalently bound by a  
carbon-carbon bond.

Figure S4; HPLC-APCI-MS base peak chromatograms of A) a tropical peat sample  
from Peru (the Aucayacu peatland, 330 cm depth), B) sample from the Champagne  
pool hot spring, and C) acid-hydrolyzed extract of the extremophile *Thermoplasma*  
*acidophilum*.

Figure S5; HPLC-APCI-MS base peak chromatograms of A) a tropical peat sample  
from Peru (the Aucayacu peatland, 330 cm depth) and B) co-injection of the tropical

peat sample with the acid-hydrolyzed extract of the extremophile *Thermoplasma acidophilum* that contains *iso*GDGT-5 but not crenarchaeol.

Figure S6; Fractional abundance of the individual *iso*GDGTs versus peat pH. Horizontal bars reflect range of peat pH<sup>S43</sup>, while vertical bars represent 1 $\sigma$  from the average fractional abundance and are based on the analysis of multiple samples from the same peatland. Fractional abundances < 0.001 are not shown.

Figure S7; Relative abundance of *iso*GDGT-5 (%) versus A) calcium content (a measure of pH) for individual samples in a range of tropical peatlands from Peru that all experience the same climate. (Ca content from<sup>S48,49</sup>) and B) CBT<sub>peat</sub>-based pH. Note that Ca data is not available for every sample.

Figure S8; Downcore relative abundance of *iso*GDGT-5 (%, orange) and calcium content (mg/kg, blue) in the 750 cm long peat core from the Aucayacu peatland in Peru that spans the last 9 kyr. Pie charts reflect the relative distribution of *iso*GDGTs in the top and bottom of the peat. (Radiocarbon ages from<sup>S50</sup>)

Figure S9; A) Ring index and B) TEX<sub>86</sub> versus peat pH. Horizontal bars reflect range of peat pH<sup>S43</sup>, while vertical error bars represent 1 $\sigma$  from the average and are based on the analysis of multiple samples from the same peatland.

Figure S10; Fractional abundance of the individual *iso*GDGTs versus overlying mean annual air temperature. Vertical error bars represent 1 $\sigma$  from the average fractional abundance and are based on the analysis of multiple samples from the same peatland. Samples with a fractional abundance < 0.001 are not shown.

Figure S11; A) Ring index and B) TEX<sub>86</sub> versus mean annual air temperature. Vertical error bars represent 1 $\sigma$  from the average and are based on the analysis of multiple samples from the same peatland.

Figure S12; HPLC-APCI-MS base peak chromatograms highlight the *iso*- and *br*GDGT distribution in A) early Paleogene lignite from UK (Cobham CL70, 11.95 cm), B) modern mid-latitude peat samples from Germany (Bissendorfer Moor, 18 cm



depth), and C) modern tropical peat sample from Peru (the Aucayacu peatland, 330 cm depth). Modern MAAT Bissendorfer Moor and Aucayacu are 8.9 °C and 26 °C, while pH for these peats is 4 and 3.7, respectively.

Figure S13; Ternary plot of the *br*GDGT-distribution in the modern peat database<sup>S43</sup> and all early Paleogene lignites used in this study. Plot shows the relative abundance of the tetra- (*br*GDGT-Ia, -Ib, and Ic), penta- (*br*GDGT-IIa, -IIa', -IIb, -IIb', -IIc, and -IIc'), and hexamethylated *br*GDGTs (*br*GDGT-IIIa, -IIIa', -IIIb, -IIIb', -IIIc, and -IIIc').

Figure S14; Ternary plot of the *iso*GDGT-distribution in the modern peat database, marine core-top sediments<sup>S67</sup>, and all early Paleogene lignites used in this study. Plot shows the relative abundance of the *iso*GDGT with no rings (*iso*GDGT-0), *iso*GDGTs with 1 to 3 cyclopentane rings (*iso*GDGT-1, -2, and -3), and *iso*GDGT with a cyclohexane ring (crenarchaeol).

Figure S15; Same as figure 1 of the main manuscript, but including estimates based on nearest living relatives data (e.g. coexistence approach, bioclimatic analysis, etc.). Leaf physiognomy methods: K&D - Kowalski and Ditcher leaf margin analysis calibration<sup>S70</sup>; CLAMP - Climate Leaf Analysis Multivariate Program[Yang, 2011 #1991]; other leaf physiognomic - for example using alternative leaf margin analysis calibrations<sup>S71</sup>. MAAT – mean annual air temperature.

Figure S16; Same as figure 3 of the main manuscript, but including estimates based on nearest living relatives data (e.g. coexistence approach, bioclimatic analysis, etc.). For abbreviations see Figure S15.

Figure S17; Global temperature anomaly between the early Paleogene and present for all available terrestrial temperature data at the paleolatitude of each location together with the zonal mean anomaly simulated by a range of climate models; 2xCO<sub>2</sub> ECHAM5<sup>S86</sup>, 2xCO<sub>2</sub> FAMOUS<sup>S87</sup>, 4xCO<sub>2</sub> GISS<sup>S88</sup>, 5xCO<sub>2</sub> CCSM3\_K<sup>S89</sup>, 6xCO<sub>2</sub> HadCM3L<sup>S90</sup>, 16xCO<sub>2</sub> CCSM3\_W<sup>S91</sup> and 16xCO<sub>2</sub> CCSM3\_H<sup>S69</sup>.



Figure S1

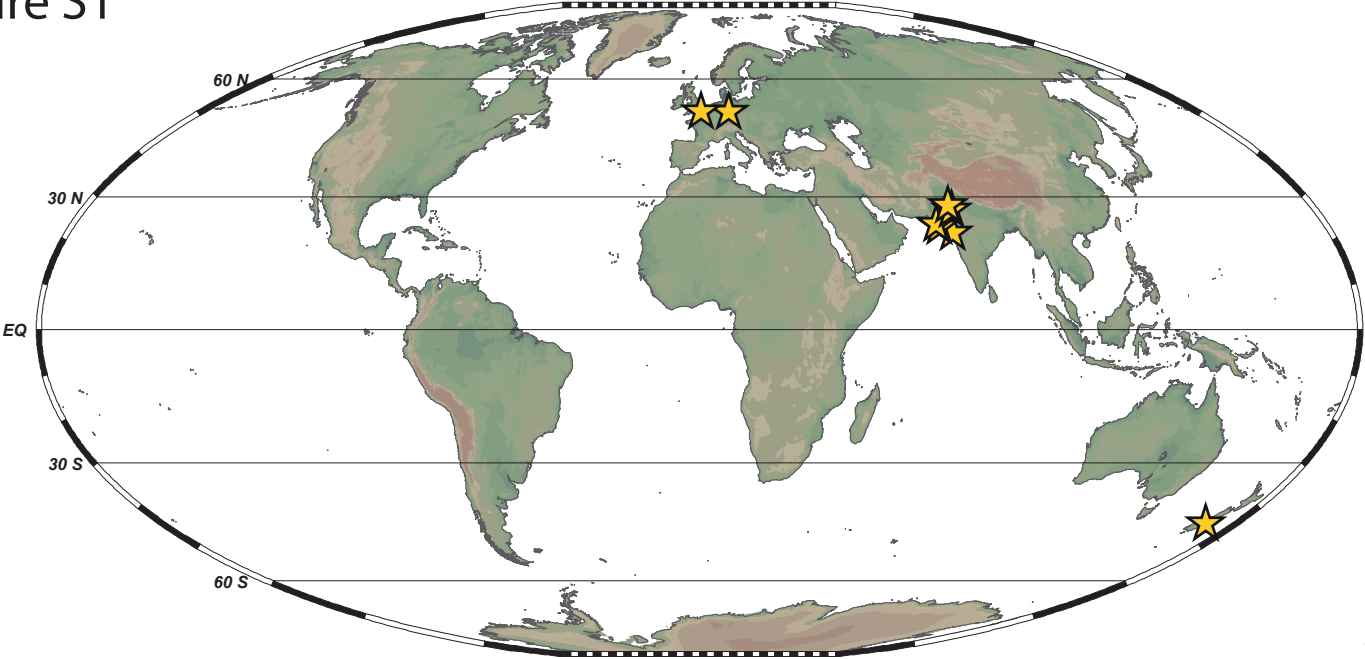


Figure S2

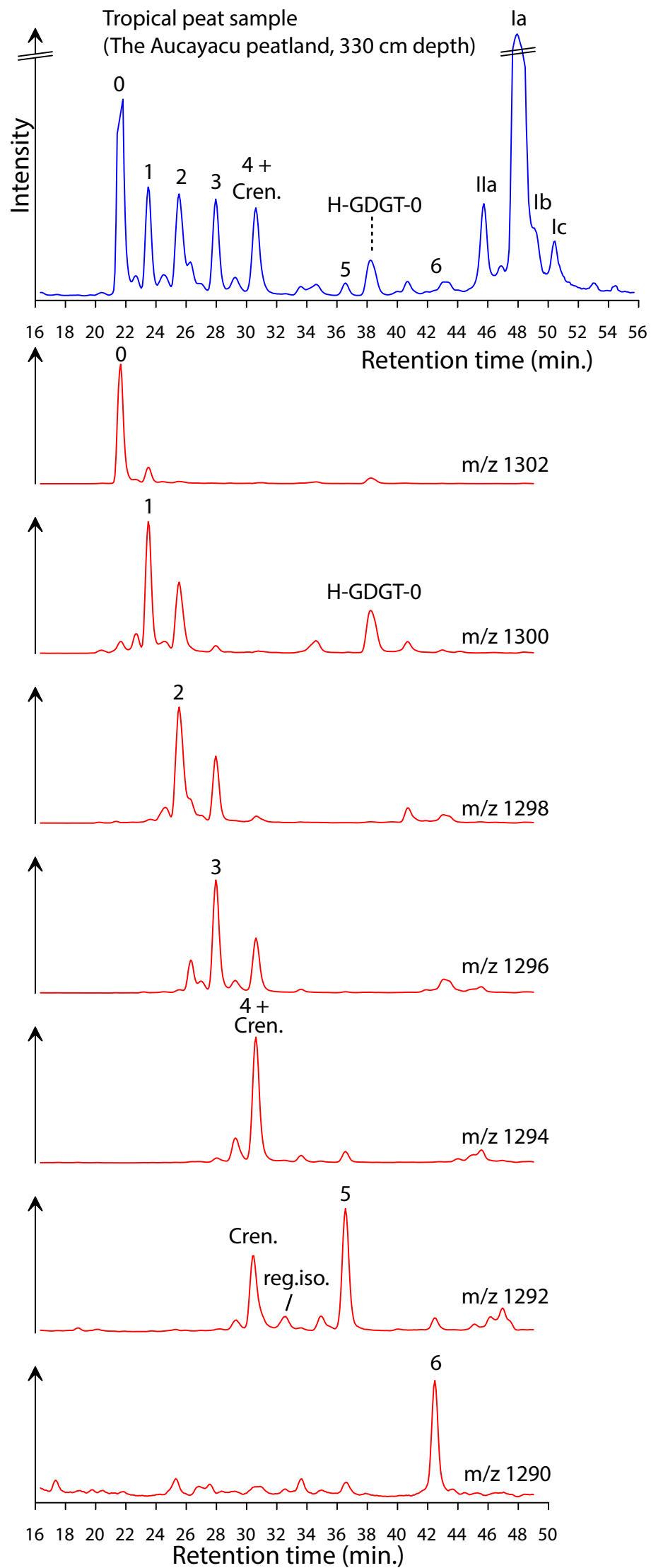


Figure S3

early Paleogene sample Cobham lignite (CL70, 11.95 cm)

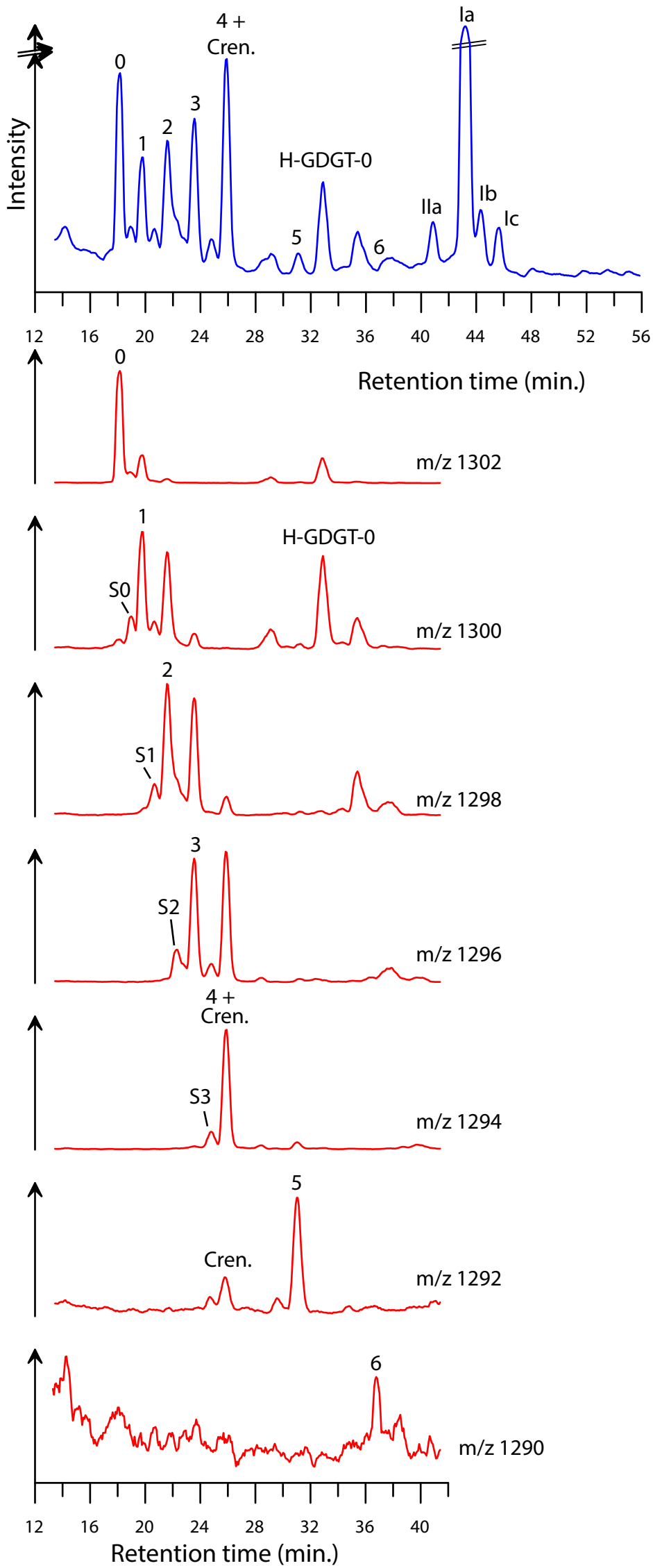


Figure S4

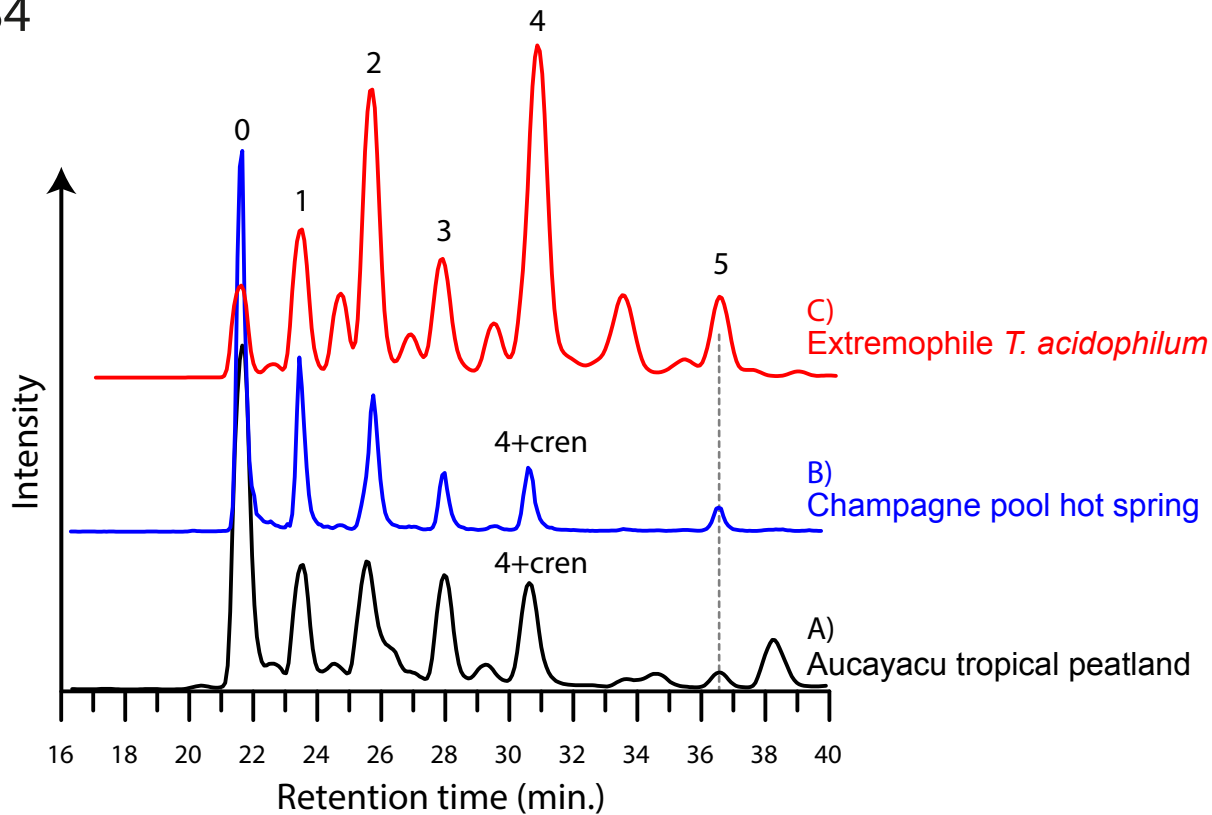


Figure S5

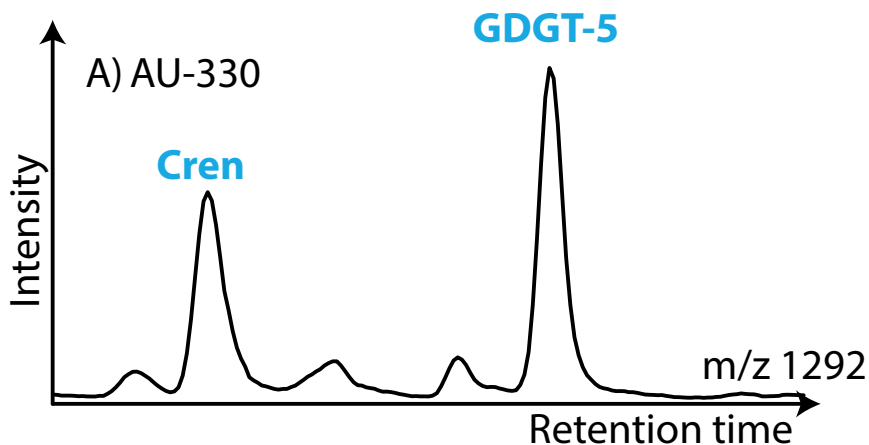
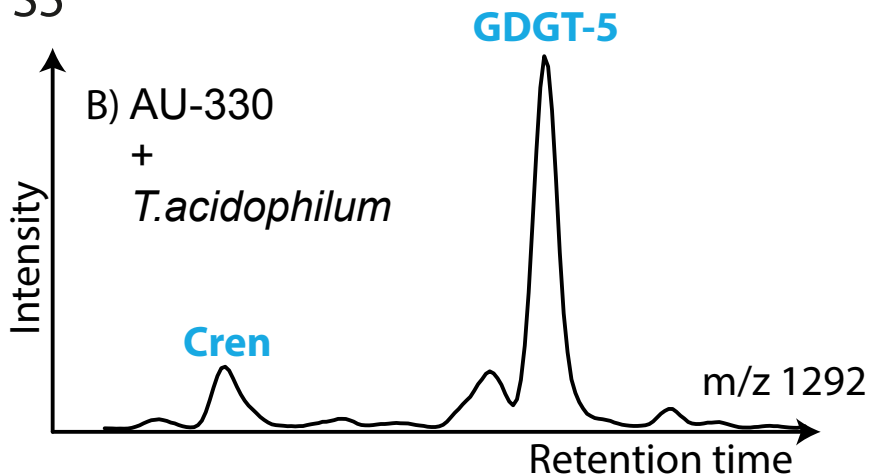


Figure S6

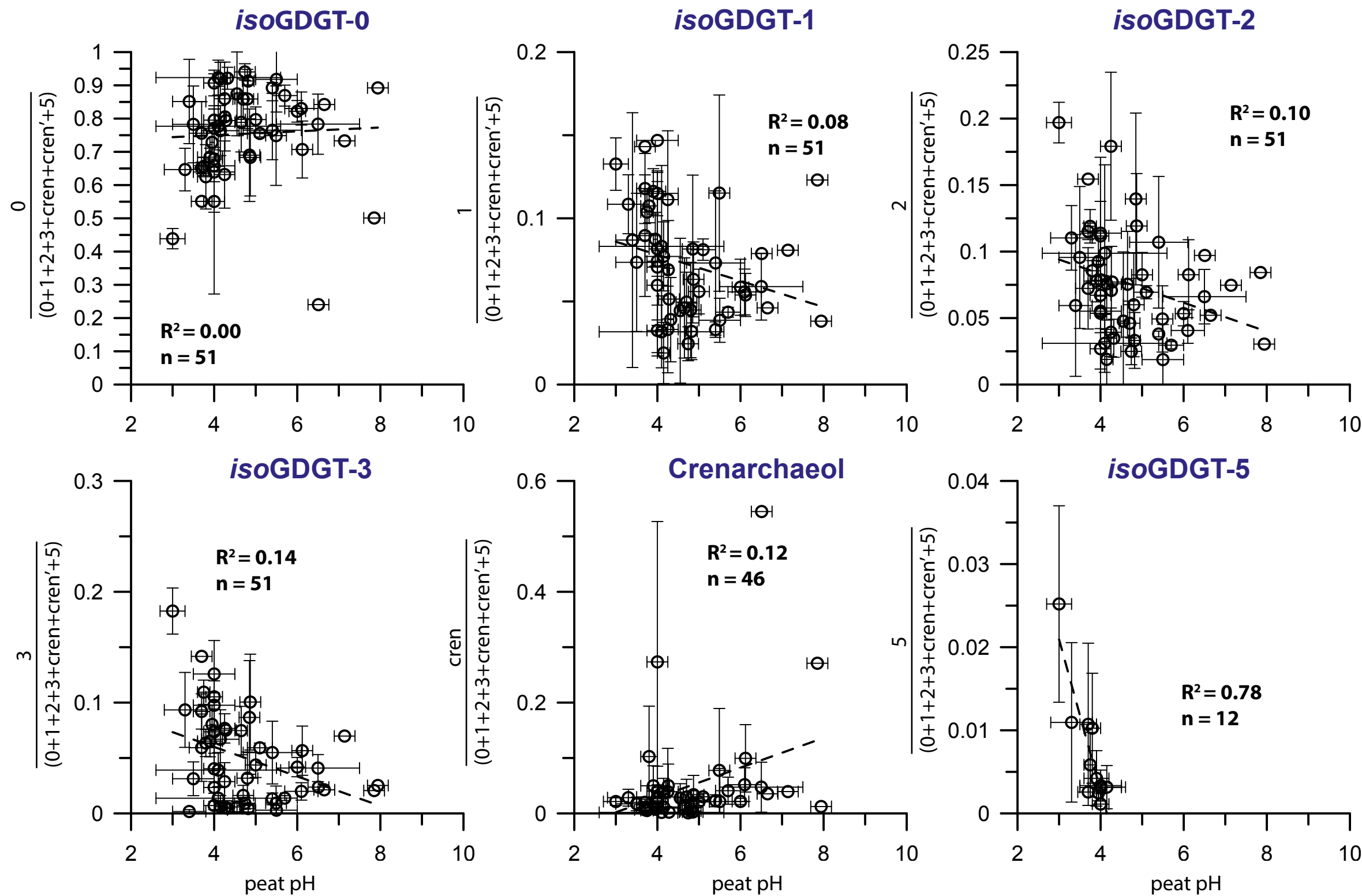
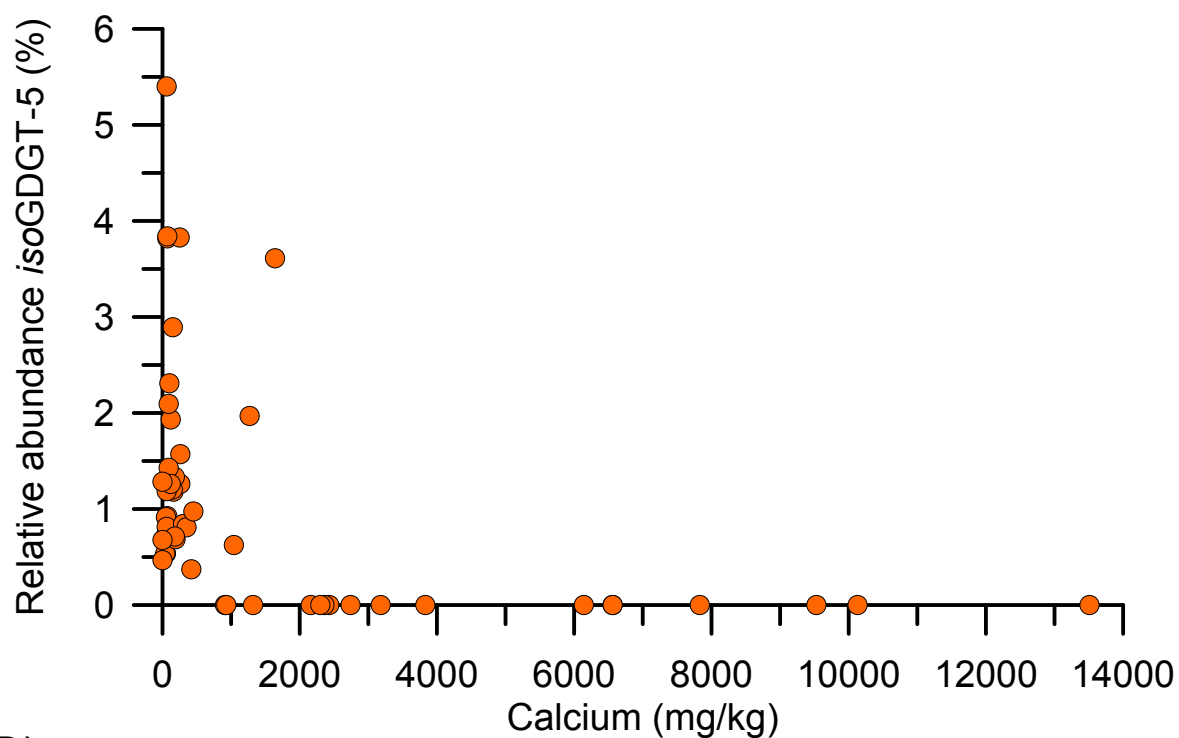




Figure S7

A)



B)

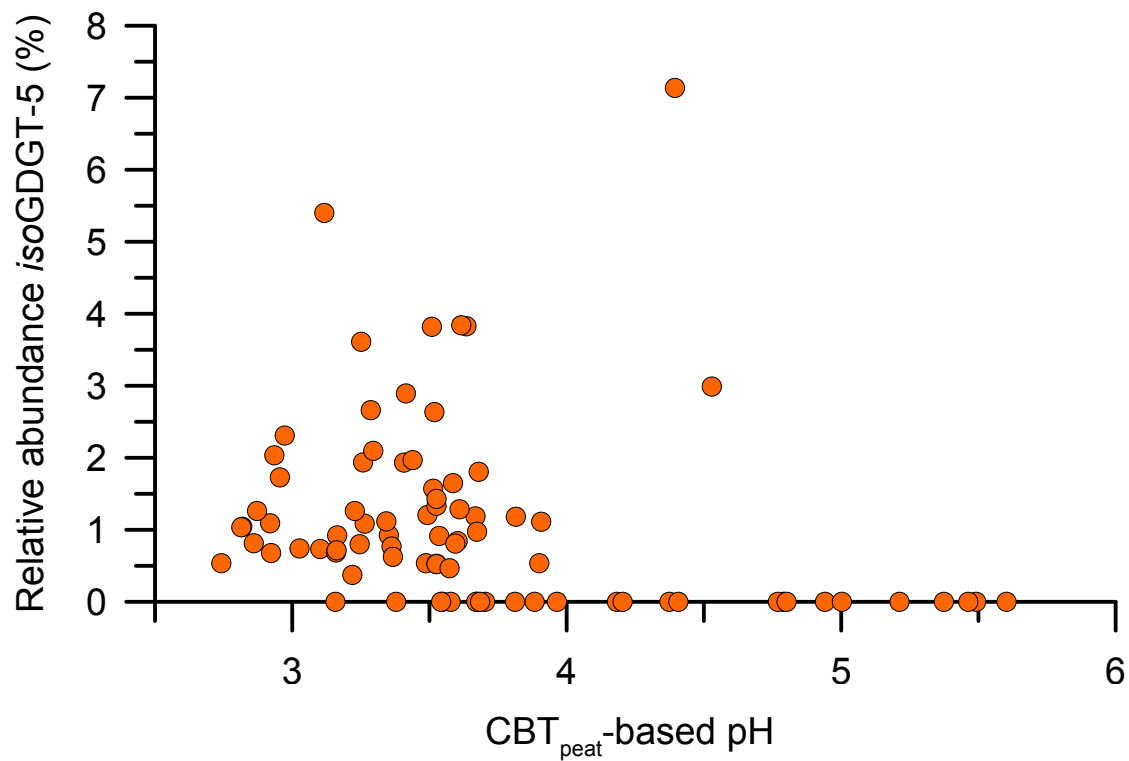


Figure S8

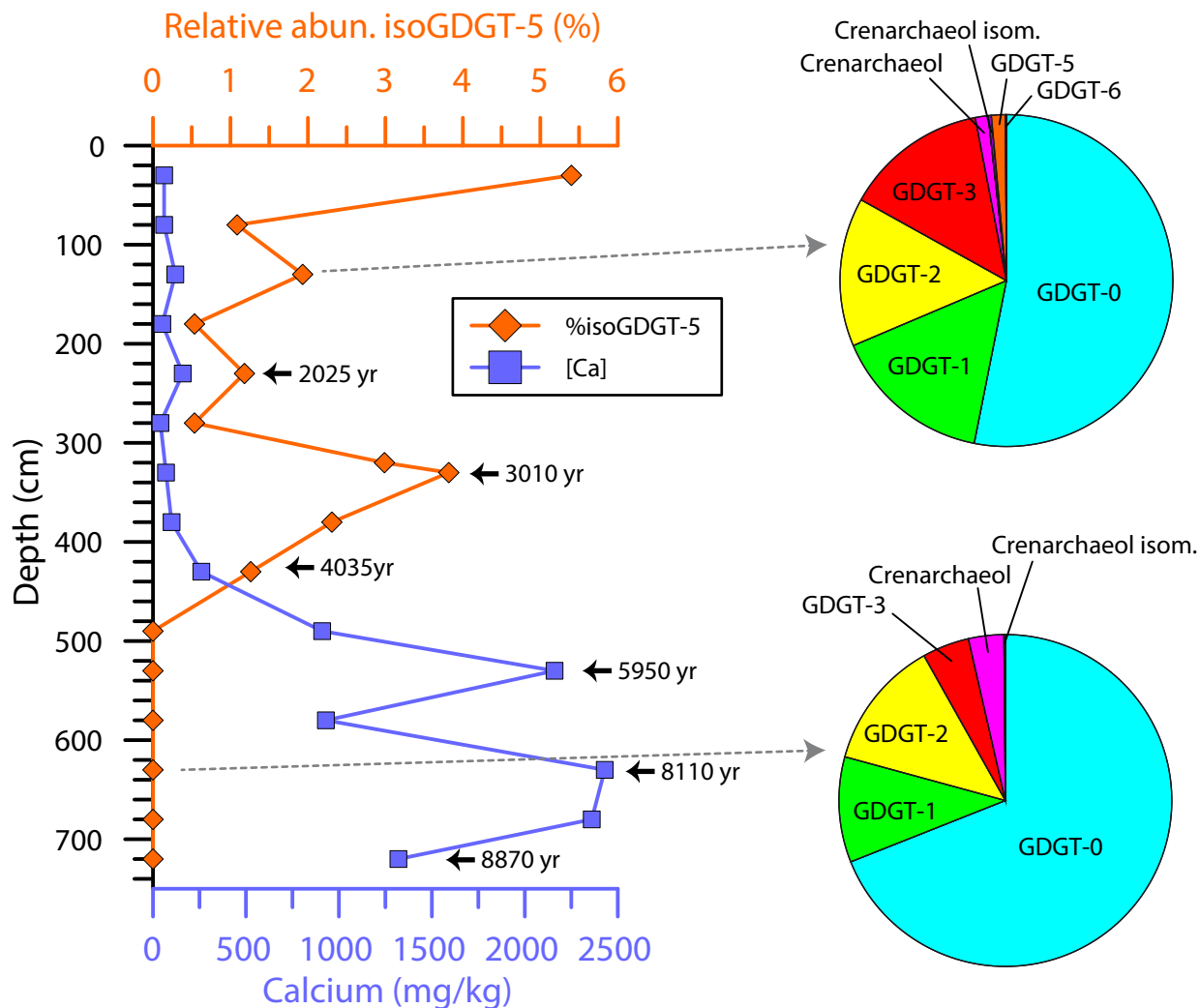


Figure S9

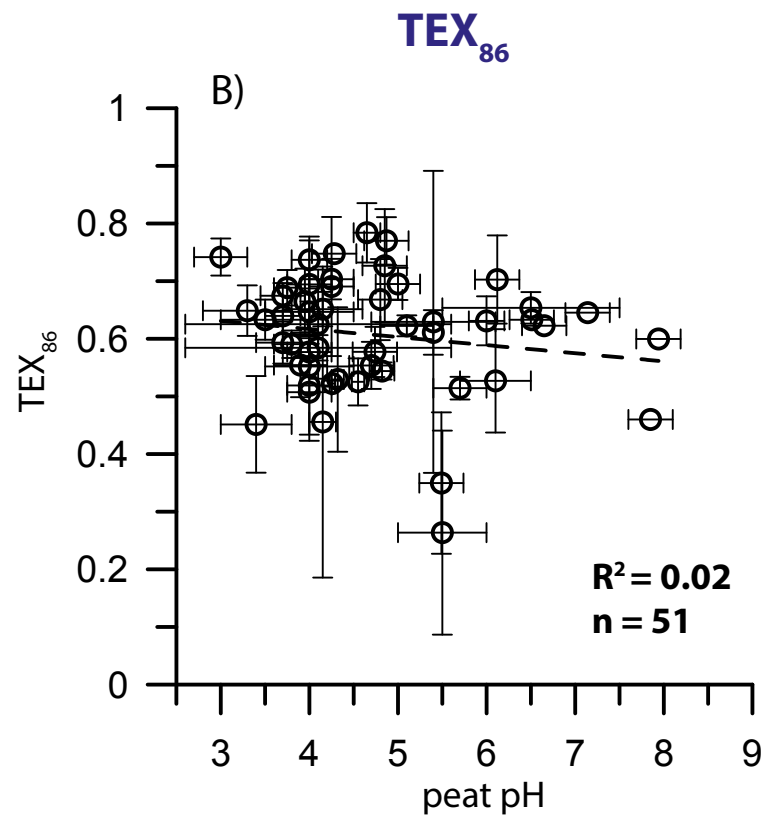
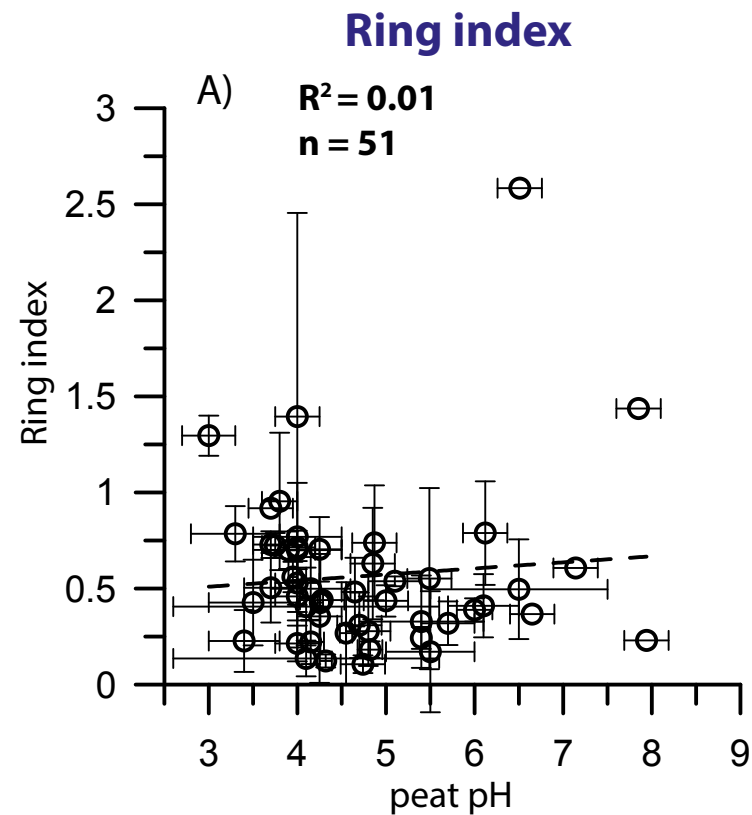


Figure S10

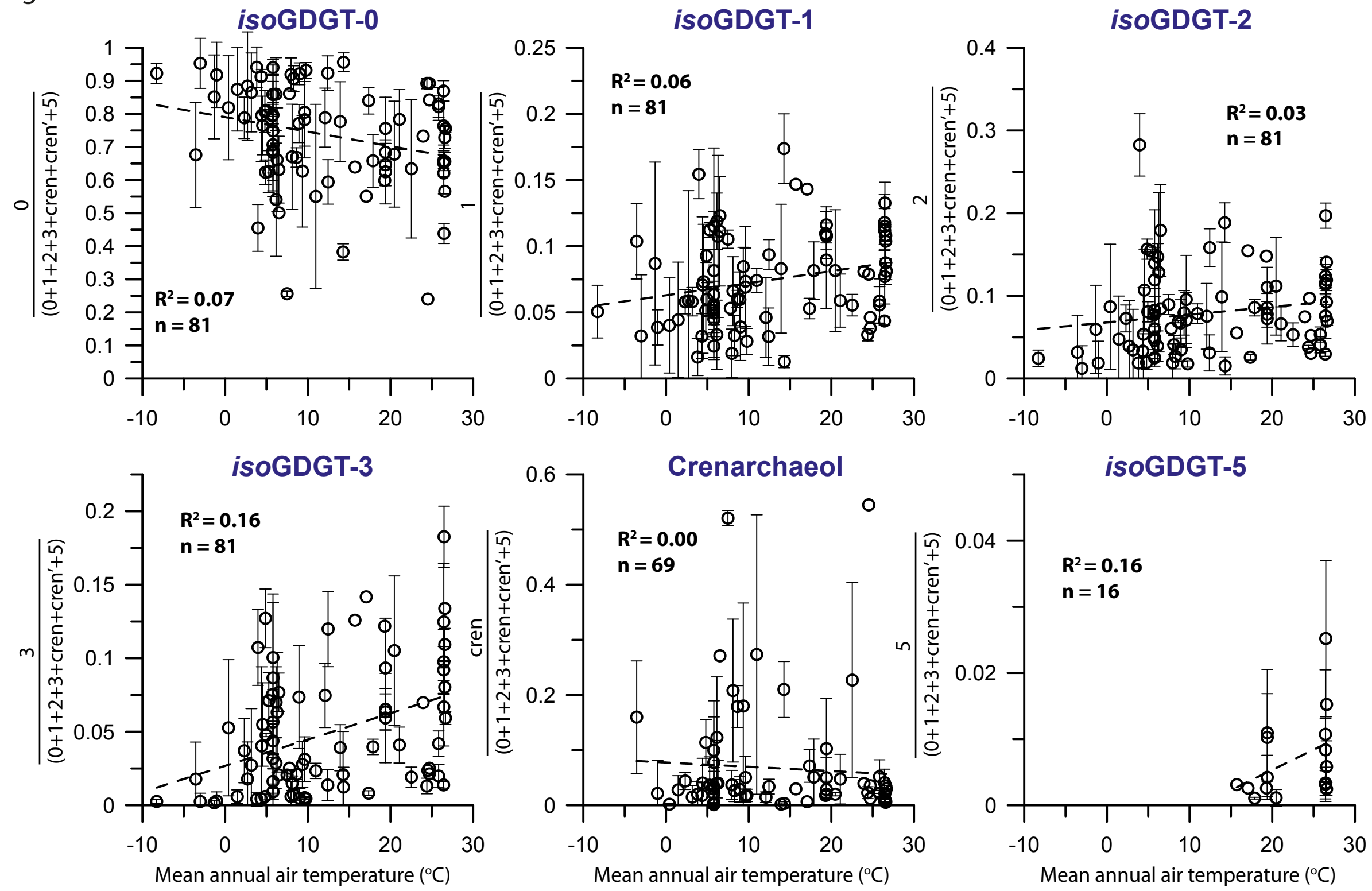


Figure S11

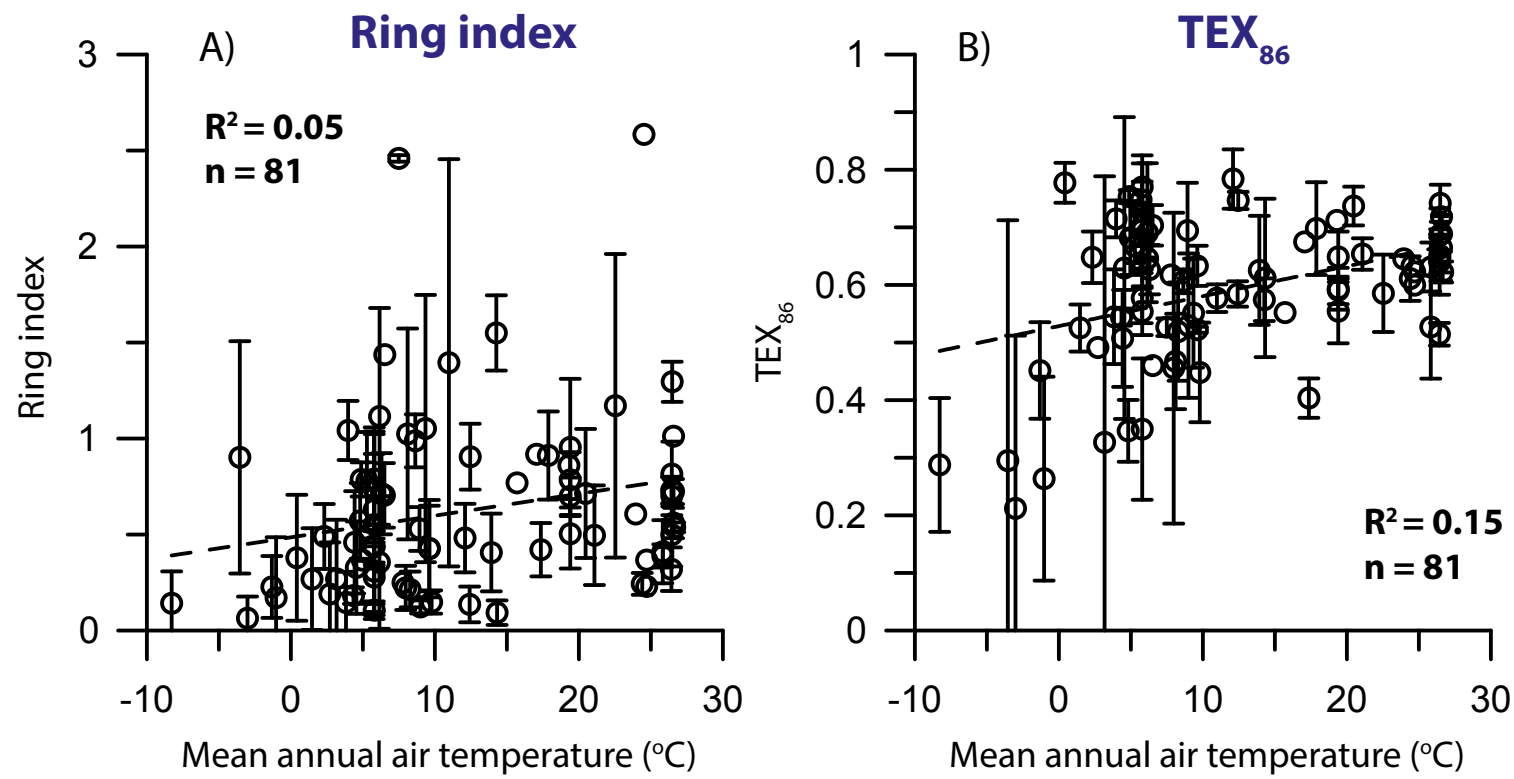


Figure S12

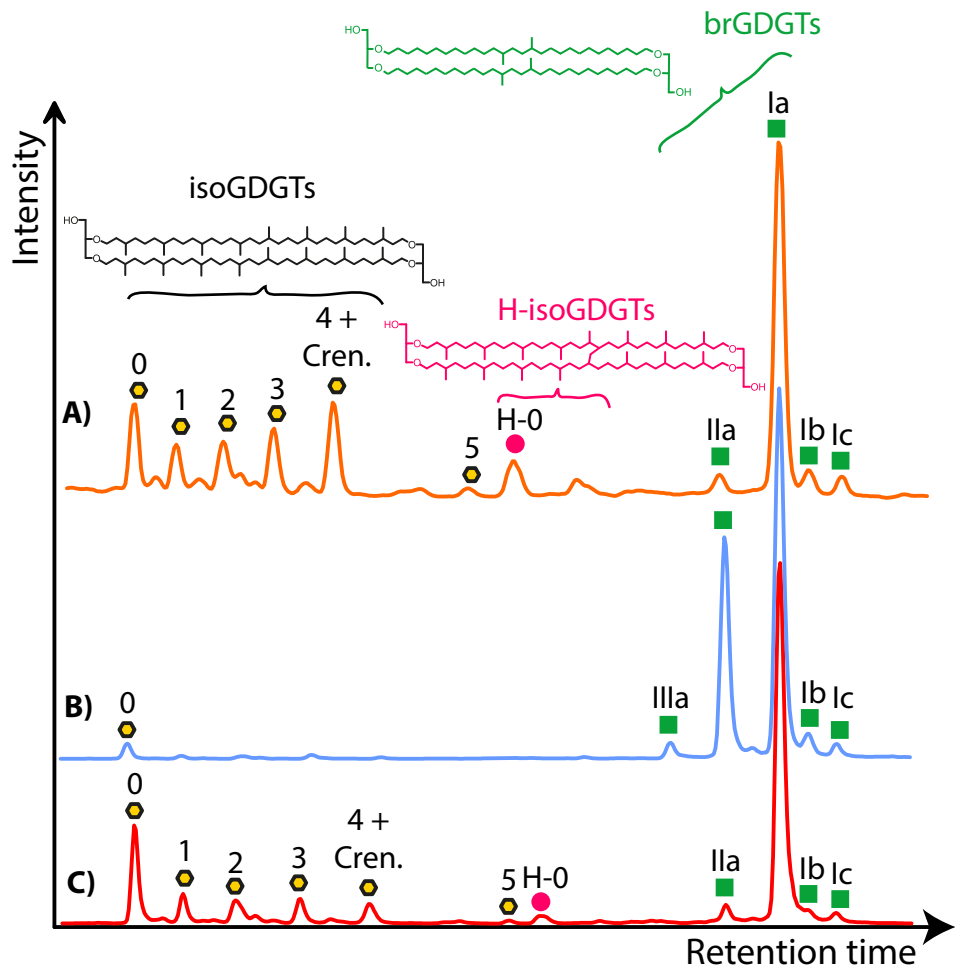


Figure S13

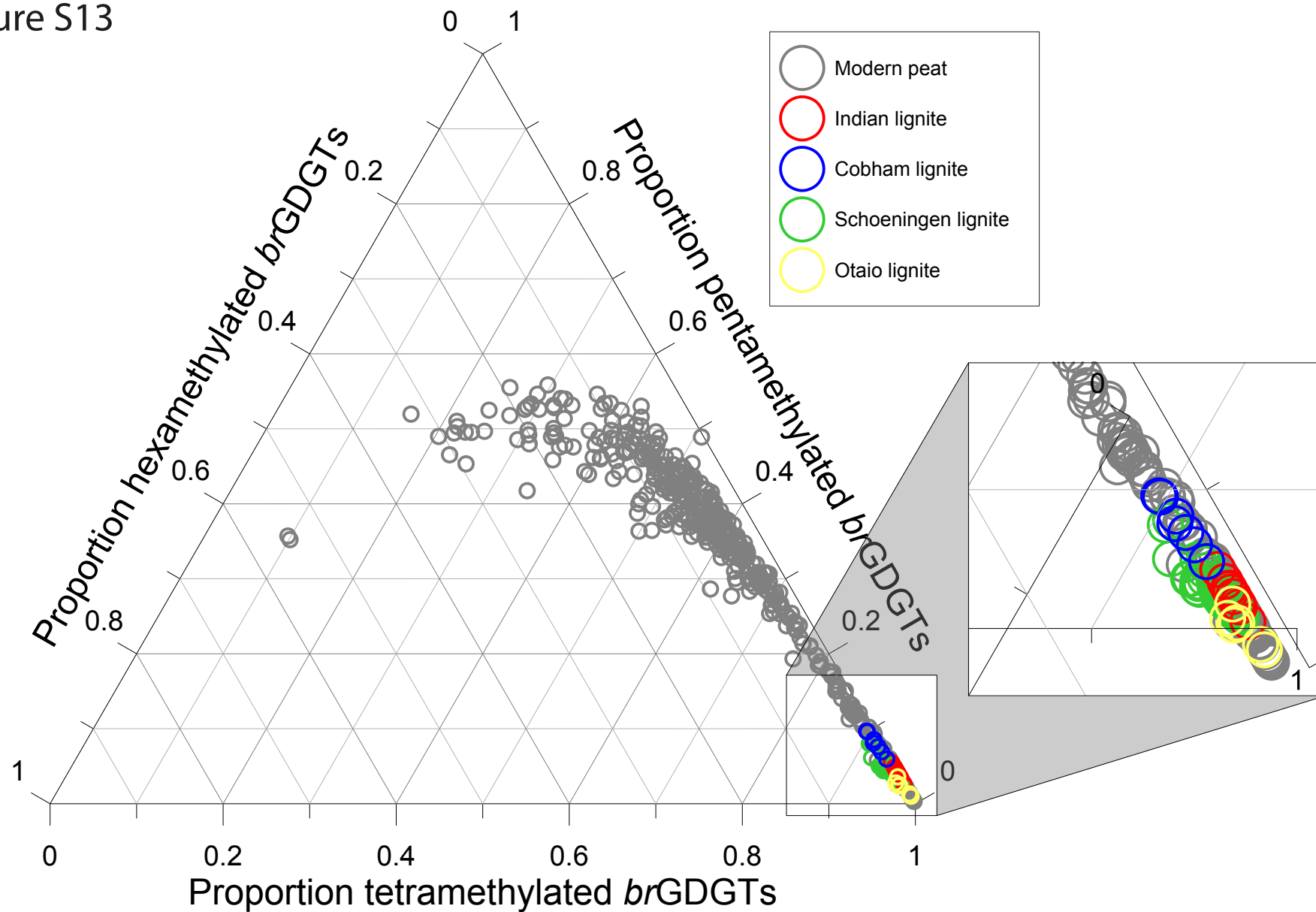


Figure S14

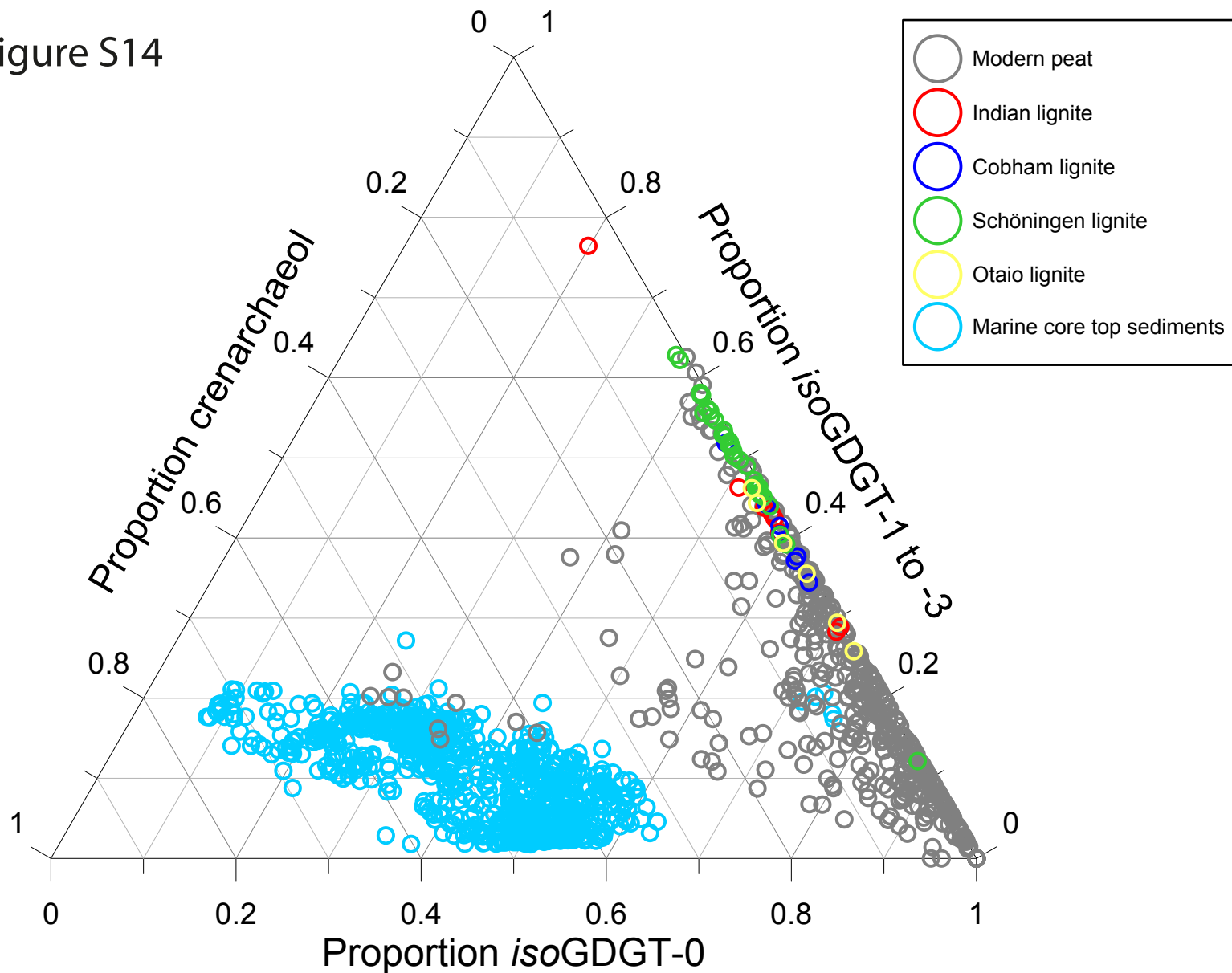




Figure S15

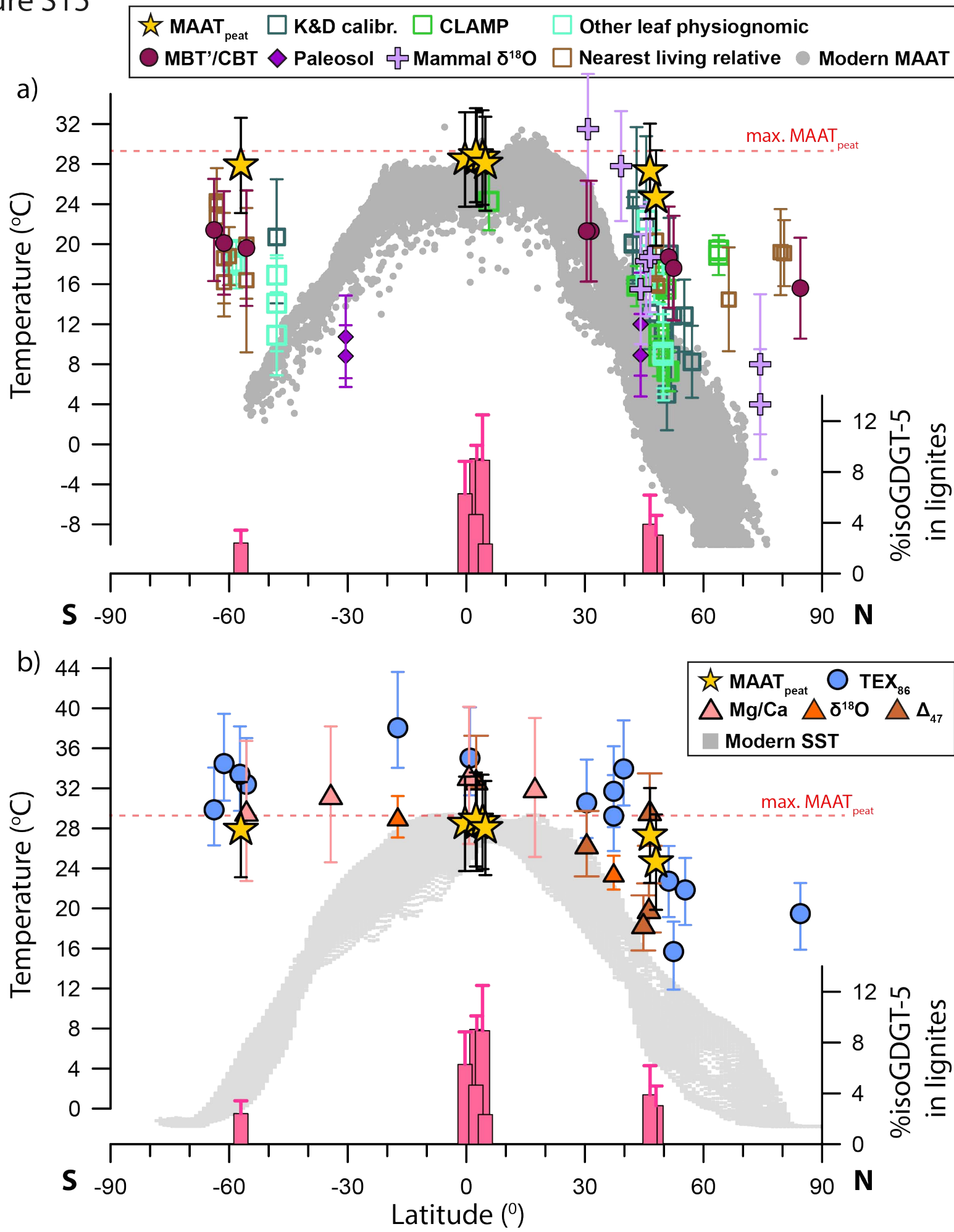


Figure S16

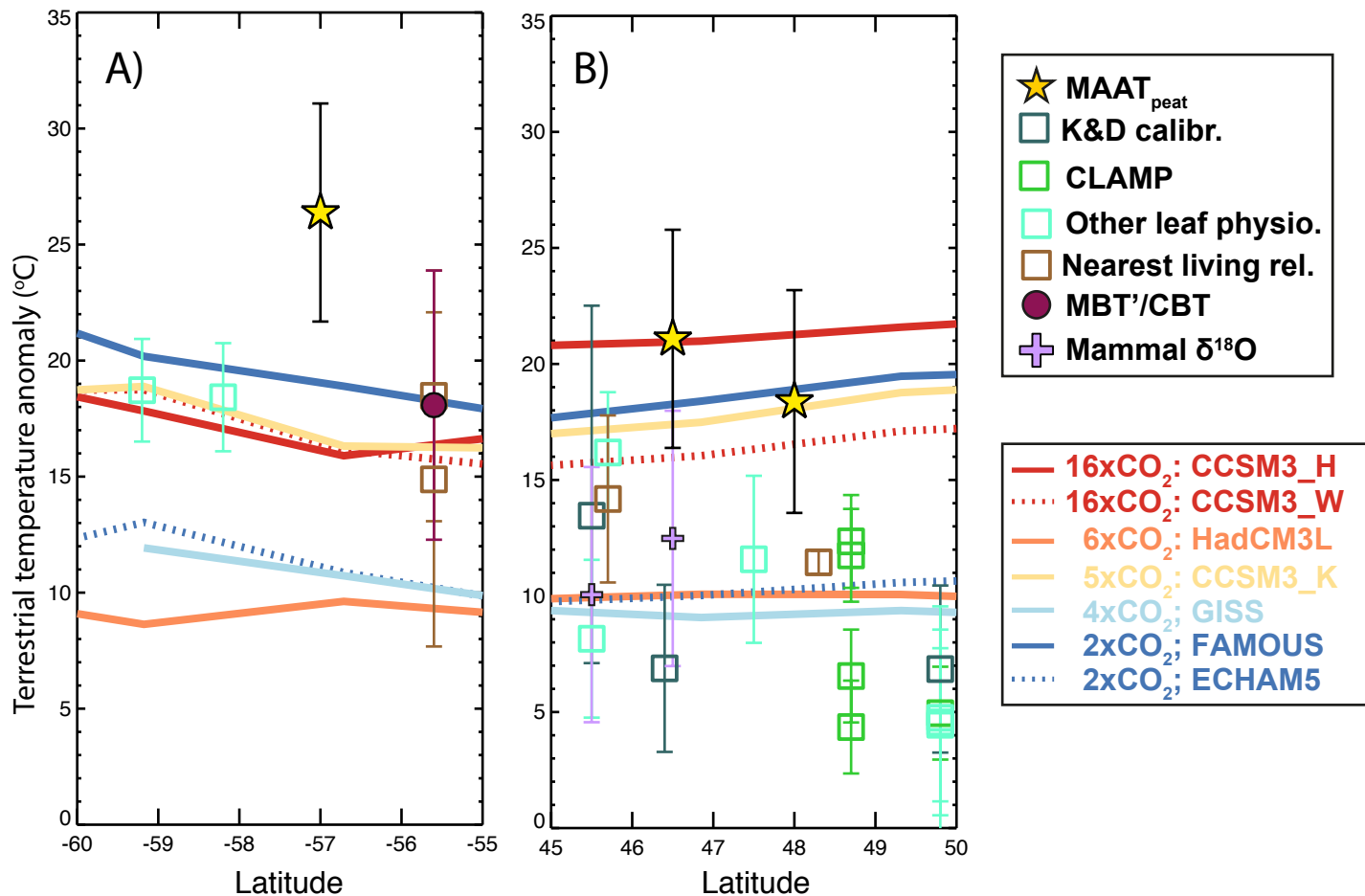


Figure S17

